frontiers | Frontiers in Earth Science

TYPE Original Research
PUBLISHED 29 July 2024
DOI 10.3389/feart.2024.1444751

Check for updates

OPEN ACCESS

EDITED BY
Feng Guo,
Chinese Academy of Sciences (CAS), China

REVIEWED BY
Xiaofeng Qin,
Guilin University of Technology, China
Yunying Zhang,
Chinese Academy of Sciences (CAS), China

*CORRESPONDENCE
Fang Liu,
liufang@lyun.edu.cn

RECEIVED 06 June 2024
ACCEPTED 08 July 2024
PUBLISHED 29 July 2024

CITATION
Lyu P, Liu F, Chen L, Song Z, Ma W and Hou Y (2024), Petrogenesis and tectonic implications of Early Paleozoic granitoids in the Baoshan deposit, Guangxi, South China. *Front. Earth Sci.* 12:1444751.
doi: 10.3389/feart.2024.1444751

Petrogenesis and tectonic implications of Early Paleozoic granitoids in the Baoshan deposit, Guangxi, South China

Puliang Lyu[1], Fang Liu[2]*, Ling Chen[3], Zhiguang Song[1], Wenen Ma[4] and Yanlin Hou[1,5]

[1]Key Laboratory of Environment Change and Resources Use in Beibu Gulf, and Institute of Geography and Oceanography, Nanning Normal University, Nanning, China, [2]School of Resource Engineering, Longyan University, Longyan, China, [3]School of Materials and Chemical Engineering, Yibin University, Yibin, China, [4]Guangxi Zhuang Autonomous Region Geophysical Survey Institute, Liuzhou, China, [5]Guangxi Geographical Indication Crops Research Center of Big Data Mining and Experimental Engineering Technology, Nanning Normal University, Nanning, China

The Early Paleozoic tectonic setting and geological processes of the South China Block have long been a subject of debate. This study presented zircon U-Pb geochronology and Hf isotope, and whole-rock geochemical analyses for the Early Paleozoic granitoids in the Baoshan deposit of the Dayaoshan Uplift. LA–ICP–MS zircon U-Pb results suggest that the diorites, granite porphyries, granodiorites and its mafic microgranular enclaves in the Baoshan deposit formed at 449–430 Ma. Their formation ages are consistent with those of granite, MMEs and mafic rocks found in the Dayaoshan region. The granite porphyries, granodiorites, diorites and their MMEs in the Baoshan deposit have high Eu/Eu*ratios, low Zr + Nb + Y + Ce contents, 10,000×Ga/Al values, and A/CNK ratios (0.74–1.08), belonging to metaluminous to weakly peraluminous calc-alkaline I-type granitoids. Based on zircon Hf isotopic compositions ($\varepsilon_{Hf}(t)$ from −5.5 to +3.1), it is unlikely that these rocks were solely originated from a crustal source, and mantle-derived magma also played a significant role in the formation of these intrusive rocks. It is inferred that the granitoids in the Baoshan deposit were probably formed through the underplating of mantle-derived magmas during a transitional collision to extension tectonic setting, which led to the remelting of Mesoproterozoic crust.

KEYWORDS

granitoids, mafic microgranular enclaves, early Paleozoic, Baoshan deposit, South China block

1 Introduction

The Dayaoshan Uplift in the eastern Guangxi Zhuang Autonomous Region is a significant component of the southwest segment of the Qin–Hang metallogenic belt in the South China Block (SCB; Figure 1A) (Faure et al., 2009; Yang et al., 2009; Ma et al., 2024). This region exhibits intense magmatic and tectonic activities, along with a broad distribution of intermediate–acidic magmatic rocks and associated W–Mo–Cu–Au–Ag–Pb–Zn deposits (Chen et al., 2011; Hu et al., 2012; Li et al., 2014; Liu et al., 2023). Recent high-precision geochronological investigations have shown that the majority of granitic plutons in this area were emplaced during the Early Paleozoic (470–430 Ma), Late Paleozoic to Early Mesozoic

(270–240 Ma), and Late Mesozoic (170–150 and 110–90 Ma) periods. Among these, mineralization associated with intermediate–acidic granitoids primarily occurred during the Early Paleozoic and Late Mesozoic periods (Wu et al., 2015; Ye et al., 2015; Jiang et al., 2017; Lyu et al., 2020; Ma et al., 2024). Nevertheless, the Early Paleozoic granitoids have received less attention in comparison to Late Mesozoic granitoids (Zhou, 2003; Guo and Liu, 2021; Ma et al., 2024). Furthermore, existing research has predominantly concentrated on Early Paleozoic S-type granitoids (Wang et al., 2007; Wang et al., 2011; Song et al., 2015), with limited emphasis on Early Paleozoic I-type granitoids. The Early Paleozoic tectonic setting of the SCB remains debated, and previous studies focused on the sedimentary provenance (Lyu et al., 2020; Gan et al., 2023). Therefore, further investigation about the Early Paleozoic intrusive rocks in this region, particularly I-type granitoids, is essential for a comprehensive understanding of the Early Paleozoic geological processes in the SCB.

The Baoshan deposit, a newly discovered copper deposit, is located in the south–central Dayaoshan Uplift (Qiu, 2021). While much research has been done on the Late Mesozoic granitoids (Bi et al., 2015; Zhang et al., 2018; Huang et al., 2019), there have been few studies on the petrogenesis and tectonic implications of Early Paleozoic intrusive rocks in the Baoshan deposit. Some of these intrusive rocks, particularly granodioritic rocks, contain abundant MMEs. These MMEs are usually considered to be indicative of magma mixing and commonly found in calc-alkaline granitic rocks (Didier and Barbarin, 1991; Cheng et al., 2009; Liu Y. et al., 2010; Chen et al., 2018). MMEs can provide important information about magma sources, petrogenetic histories, and deep magmatic processes of granitic rocks (Barbarin, 2005; Yang et al., 2007). Magmatic mixing involves significant material exchange, which can offer insights into the geochemical information of the magma source. Petrology and zircon Hf isotope evidence is often well-preserved during magma evolution and can be used to assess the occurrence of magma mixing (Janoušek et al., 2004; Hawkesworth and Kemp, 2006; Guan et al., 2016). Thus, systematic zircon geochronology and Hf isotope, and whole-rock geochemistry analyses in this study were conducted on the Early Paleozoic intrusive rocks and MMEs in the Baoshan deposit to constrain their petrogenesis and tectonic setting. The new zircon U–Pb geochronology and Hf isotopic data and whole-rock geochemical compositions help determine the timing and origin of the Early Paleozoic magmatism (Liu et al., 2024). Based on these results, this study aims to explore the characteristics of tectono-magmatic activity and tectonic setting during the Early Paleozoic era in the SCB.

2 Geological setting

Since the Late Proterozoic, the Dayaoshan Uplift has experienced multiple periods of tectonic evolution, such as the Caledonian, Hercynian, Indosinian and Yanshanian movements (Shu et al., 2023; Tang et al., 2023). These multiple tectonic movements have formed a series of regional faults in the study area, accompanied by magma emplacement and hydrothermal activities, and forming a polymetallic mineralization belt dominated by gold, silver, tungsten, molybdenum, and other minerals (Mao et al., 2013; Mao et al., 2021). The Dayaoshan Uplift has a central uplift area and a surrounding fault basin, with a total area of nearly 18,000 km^2 (Figure 1B). It is a region with a weakly metamorphosed basement primarily made up of Cambrian and minor Sinian strata. Both the Cambrian and Sinian sedimentary rocks are mainly flysch deposits with a total thickness of >9000 m, consisting of sandstone, siltstone, phyllite, and carbonaceous shale (Jiang et al., 2017). The main structures in the region include the E–W-trending Dayaoshan anticlinorium and the NE-striking Pingxiang–Dali deep fault superimposed by late N–E-, N–W- and S–N-trending structures, forming a gridded ore-controlling structure (Chen et al., 2011).

The Baoshan deposit is a part of the southwestern Shedong W–Mo ore district in Cangwu County. Neritic flyschoid outcrops in the ore district are represented by the lower Cambrian Huangdongkou Formation. This formation is composed of fine-grained sandstone and siltstone with interbedded shale and carbonaceous shale. The ore district is located at the eastern Pingxiang–Dali deep fault, with the faults in the NW direction. The NW-trending normal fault with an attitude of 215°∠80° is most closely related to diagenesis and mineralization. This fault cuts the main granodiorites body and controls the attitude of the concealed quartz porphyry body. The width of the fault is 2–10 m, extending nearly 1 km, with strong silicification (or quartz veining), pyritization, fluoritization and other alteration and mineralization, forming the ore-controlling structure of the Baoshan deposit (Jiang et al., 2015).

The Baoshan pluton intruded into Cambrian strata and consists of granodiorites and granite porphyries. The pluton extends in a NW direction with 3 km in length and 1 km in width. The granodiorites contain abundant MMEs, quartz-vein-type scheelite and galena mineralization, and a small amount of molybdenite mineralization (Jiang et al., 2017). The granite porphyries have an intrusive contact with the granodiorites (Figure 1C). The Baoshan deposit is small in size, with Cu concentrations of 0.2%–3.1%, Pb concentrations of 1.1%–4.9% and Zn concentrations of 0.8%–4.1% (Huang et al., 2019).

3 Sample descriptions and analytical methods

3.1 Sample descriptions

The granite porphyry samples were collected from borehole ZK28003, granodiorite samples from boreholes ZK28805 and ZK28003, diorite dyke samples from borehole ZK1108, and MMEs samples from boreholes ZK28805 and ZK1108 in the Baoshan deposit.

The granite porphyry samples are greyish white in color and show a porphyritic texture (Figure 2J–I). The phenocrysts are composed of plagioclase (~30%), K-feldspar (40%), quartz (~30%), and the fine-grained microcrystalline matrix have similar mineralogy associations. Plagioclase crystals are granular or short–prismatic in shape, ranging from 1.0 to 2.0 mm in size, and some of them have undergone strong sericitization. K-feldspar crystals are tabular and 2.0–3.5 mm in size. Quartz crystals are granular and 1.0–2.0 mm in size, and biotites are 1.0–2.0 mm in size.

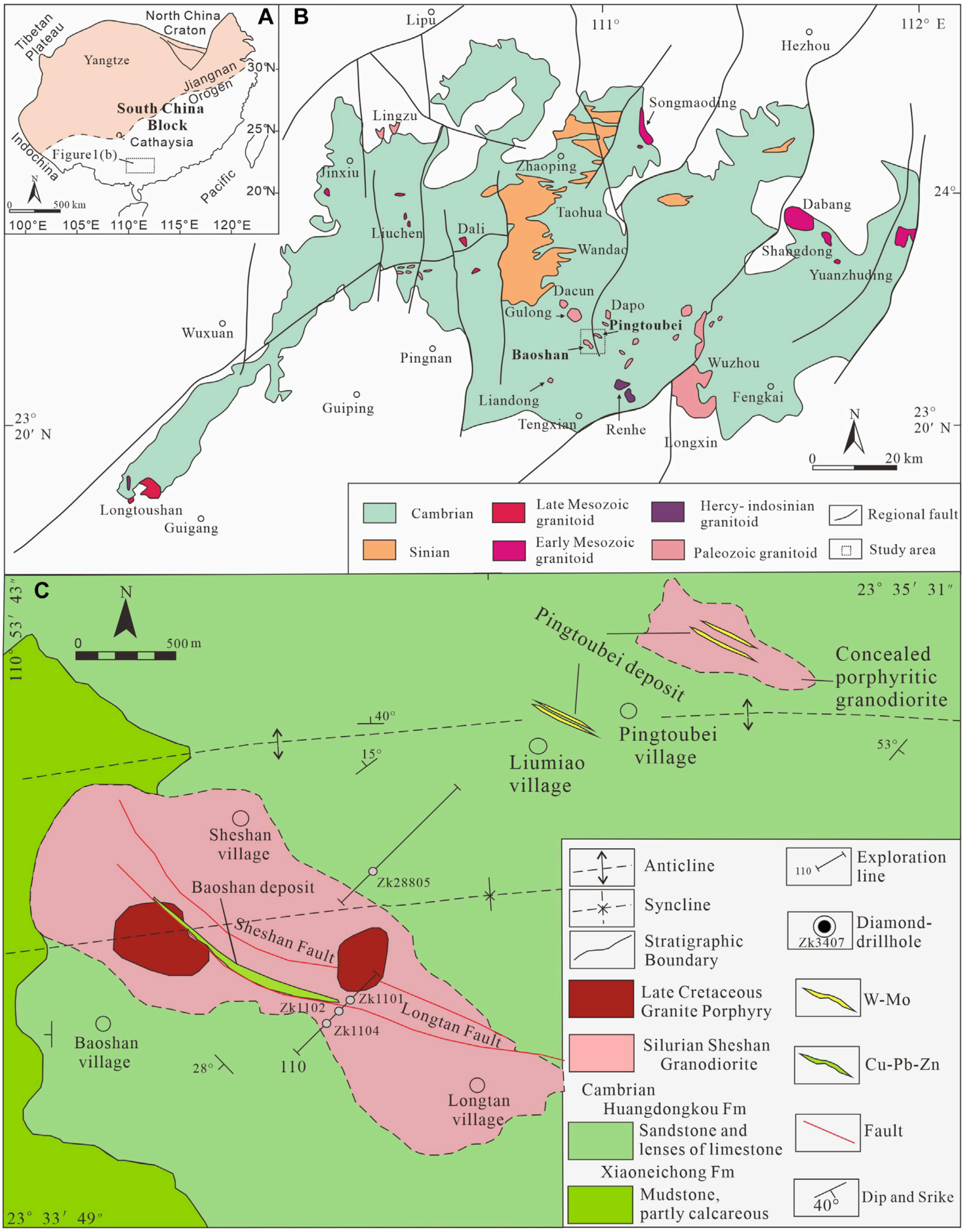

FIGURE 1
(A) Tectonic sketch map of the SCB (modified after Faure et al., 2009). **(B)** Sketch map of the Dayaoshan Uplift (modified after Chen et al., 2015). **(C)** Geological sketch map of the Baoshan Cu-Pb-Zn deposit (modified after Chen et al., 2011).

The granodiorite samples are characterized by dark grey in color, fine-to medium-grained texture, and massive structure (Figures 2G–I). It primarily consists of plagioclase (45%), quartz (~35%), hornblende (5%), and biotite (~15%). Plagioclase crystals are granular or short–prismatic in shape and generally 0.5–2.0 mm long. Quartz is granular and broadly the same size as plagioclase. Both biotite and hornblende range in size from 0.5 to 2.0 mm. The granodiorite samples contain a lot of MMEs (Figure 2G).

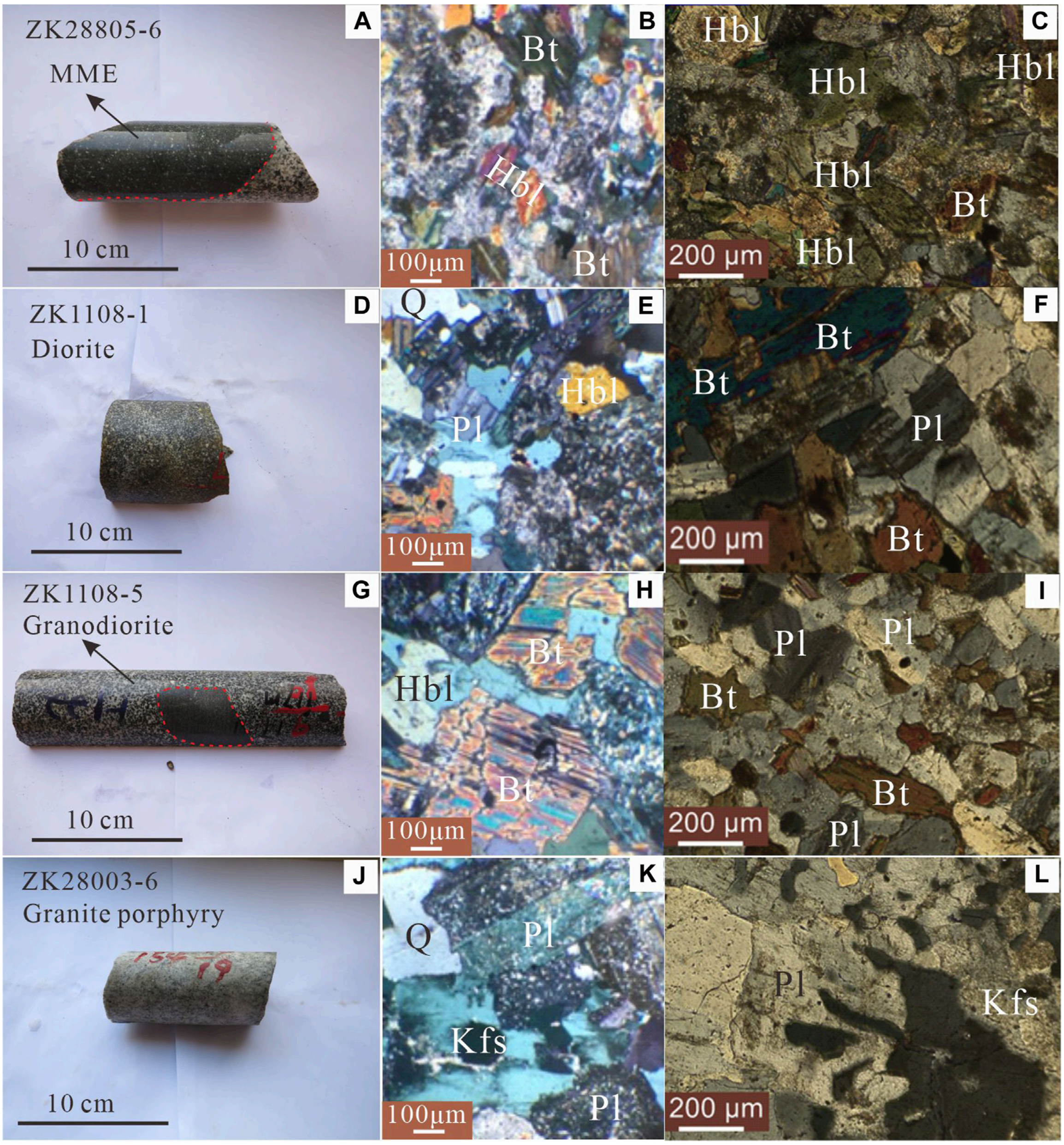

FIGURE 2
Detailed microphotographs showing **(A)** the contact relationship between granodiorites and the MMEs; **(B, C)** representative photomicrographs of the MMEs (b = cross-polarized light; c = plane-polarized light); **(D)** diorite hand specimens from the borehole; **(E, F)** photomicrographs of the diorites (e = cross-polarized light; f = plane-polarized light); **(G)** the contact relationship between granodiorites and the MMEs; **(H, I)** representative photomicrographs of the granodiorite (h = cross-polarized light; i = plane-polarized light); **(J)** hand specimens of granite porphyry from the borehole; **(K, L)** photomicrographs of the granite porphyry (k = cross-polarized light; l = plane-polarized light). Bt = biotite; Hbl = hornblende; Pl = plagioclase; Kfs =K-feldspar; Q = quartz.

Diorite dyke samples in the deposit exhibit a dark grey in color, fine- to medium-grained texture, and massive structure (Figures 2D–F). They are composed of plagioclase (45%), hornblende (~25%), biotite (15%), and quartz (~15%). Plagioclase crystals are granular and 1.0–2.0 mm in size. Quartz is granular and broadly the same size as plagioclase. Biotite and hornblende range in size from 0.2 to 2.0 mm.

Many MMEs are visible in the granodiorite samples. The MMEs are black, irregular, elliptical or lenticular in shape, 5–20 cm in length (up to 50 cm). They typically display sharp contacts with their host rocks and have weak chilled margins (Figures 2A–C). The MMEs are dominated by hornblende (40%), biotite (~27%), plagioclase (20%), and quartz (~10%), with subordinate accessory minerals (e.g., apatite and zircon). In comparison to the host granodiorites, MMEs are obviously enriched in dark mafic minerals, such as hornblende and biotite.

3.2 Zircon U-Pb dating geochronology and Lu-Hf isotope analyses

Zircons were separated using heavy liquid and magnetic techniques and then purified by hand picking under a binocular microscope. Sample grains were selected randomly, mounted in epoxy, and polished for further analysis. The internal structures of the zircons were examined using cathodoluminescence (CL) imaging prior to isotopic analysis.

Zircon U-Pb dating and *in situ* trace element analyses were simultaneously performed with an Agilent 7500a inductively coupled plasma–mass spectrometry (ICP-MS) instrument coupled with a Resonetics Resolution M-50 (193 nm ArF excimer) laser ablation (LA) system at the State Key Laboratory of Isotope Geochemistry, Guangzhou Institute of Geochemistry, Chinese Academy of Sciences (GIGCAS). Sample mounts were placed in a specially designed double volume sample cell flushed with Ar and He. The laser beam was set to 30 μm, 2 J·cm^{-2} and 5 Hz for the diameter, energy density and repetition rate, respectively. The ablated material was carried by He–Ar gas via a Squid system to homogenize the signal into the ICP–MS instrument. Each analysis incorporated a background acquisition time of approximately 20–30 s (gas blank) followed by 50 s of data acquisition during ablation. Detailed analytical procedures followed those described by Liu Y. S. et al. (2010). Off-line selection and integration of background and analyzed signals and time-drift correction and quantitative calibration for trace element analyses and U-Pb dating were performed using the in-house program ICPMSDataCal 8.3 (Liu Y. S. et al., 2010). Zircon 91,500 was used as an external standard, and zircon GJ-1 was used as an internal standard for U-Pb dating. Time-dependent drift of U–Th–Pb isotopic ratios was corrected using linear interpolation every five analyses and was monitored using variations in zircon 91,500. The obtained mean $^{206}Pb/^{238}U$ ages of 91,500 and GJ-1 are within experimental error of their recommended values (Jackson et al., 2004). The absolute abundances of U, Th and rare earth elements (REEs) were determined using an external standard glass NIST SRM 610, and ^{29}Si was used as the internal standard. Concordia diagrams and weighted mean calculations were made using Isoplot (V. 3.0) (Ludwing, 2003).

In situ zircon Lu-Hf isotopic analyses were carried out with a Neptune Plus multicollector (MC)-ICP-MS equipped with an ArF excimer laser ablation system at the State Key Laboratory of Geological Process and Mineral Resources, China University of Geosciences, Wuhan. Zircons were ablated with a laser beam with a diameter of 44 μm, laser repetition rate of 10 Hz, and laser energy of 15 J·cm^{-2}. The aerosol was carried by He gas to the MC-ICP-MS system. Based on an exponential law, instrumental mass bias corrections of Yb and Hf isotope ratios were performed by normalizing $^{172}Yb/^{173}Yb$ by 0.7325 and $^{179}Hf/^{177}Hf$ by 0.7325 (Patchett et al., 1982; Huang and Wang, 2019), respectively. Two reference standards were also analyzed during the Hf isotopic analyses: the 91,500 zircon and Penglai zircon. Raw data for Hf isotopic analyses were reduced using software ICPMSDataCal (Liu Y. S. et al., 2010) and the results are reported with 1σ error.

3.3 Whole-rock major and trace element analyses

For major and trace element analyses, the fresh whole-rock chips were cleaned and crushed to 200 mesh in an agate mill. The loss on ignition (LOI) was determined after heating the samples to 1,000 C for 3 h. Major element contents were measured by X-ray fluorescence (XRF) spectrometry on fused glass beads using a Rigaku 100e spectrometer at the ALS Laboratory group. The precision for major elements was better than 1%. Details of the XRF procedures are described by Li et al. (2005). The trace element contents were measured by a Finnigan MAT ELEMENT magnetic sector ICP-MS with precision better than 10% at the ALS Laboratory group. The details of the analytical procedure are outlined in Qi et al. (2000). International standard AMH-1 (Mount Hood andesite) (Thompson et al., 1999) was used as the standard for quality control.

4 Results

4.1 Zircon U–Pb geochronology and trace elements

Zircon U–Pb isotopic data for samples ZK28003-6 (granite porphyries), ZK28805-2 (granodiorites), ZK1108-1 (diorites), and ZK28805-6 (MMES) are presented in Supplementary Table S1. Zircon grains from samples ZK28003-6, ZK28805-2, and ZK1108-1 are mostly granular or prismatic, 50–200 μm in length and have length-to-width ratios of 1:1–4:1. The zircon grains show obvious magmatic oscillatory zoning, some of which have inherited cores or narrow accretion edges (Figure 3). The analytical results show that REEs exhibit light rare earth elements (LREEs)-depletion patterns, with significant negative Eu anomalies (av. of 0.26, 0.32, and 0.40) and high Th/U ratios (0.16–1.22, 0.44–1.02, and 0.36–0.94), which are much higher than Th/U ratios of metamorphic zircons (<0.07), indicating that plagioclase fractionation occurred in these magmas and that these zircons are typical magmatic zircons (Hoskin and Schaltegger, 2003). After excluding discordant and inherited ages, 18 grains from sample ZK28003-6 plot on or near a U–Pb concordia line, yielding a weighted mean $^{206}Pb/^{238}U$ age of 444.6 ± 6.8 Ma (MSWD = 0.81) (Figures 3C, G). Similarly, 20 grains from sample ZK28805-2 yield concordant $^{206}Pb/^{238}U$ ages, with a weighted mean age of 448.4 ± 5.7 Ma (MSWD = 0.26) (Figures 3B, F), and 7 grains from sample ZK1108-1 yield concordant $^{206}Pb/^{238}U$ ages, with a weighted mean age of 430.7 ± 8.8 Ma (MSWD = 1.19) (Figures 3D, H). These results indicate that the granite porphyry and granodiorites of the Baoshan deposit formed in the Late Ordovician and the diorites of the Baoshan deposit formed in the Early Silurian.

Zircon grains from MMEs (sample ZK28805-6) are mostly long–prismatic or granular and darker than the zircon grains in host granodiorites. These zircons are 50–250 μm in length and have length-to-width ratios of 1:1–5:1. The zircon grains show obvious magmatic oscillatory zoning. The analytical results show that REEs exhibit listric-shaped LREE-enriched patterns, without obvious negative Eu anomalies (av. of 0.91) and high Th/U ratios (0.73–1.66), indicating that limited plagioclase fractionation occurred in the

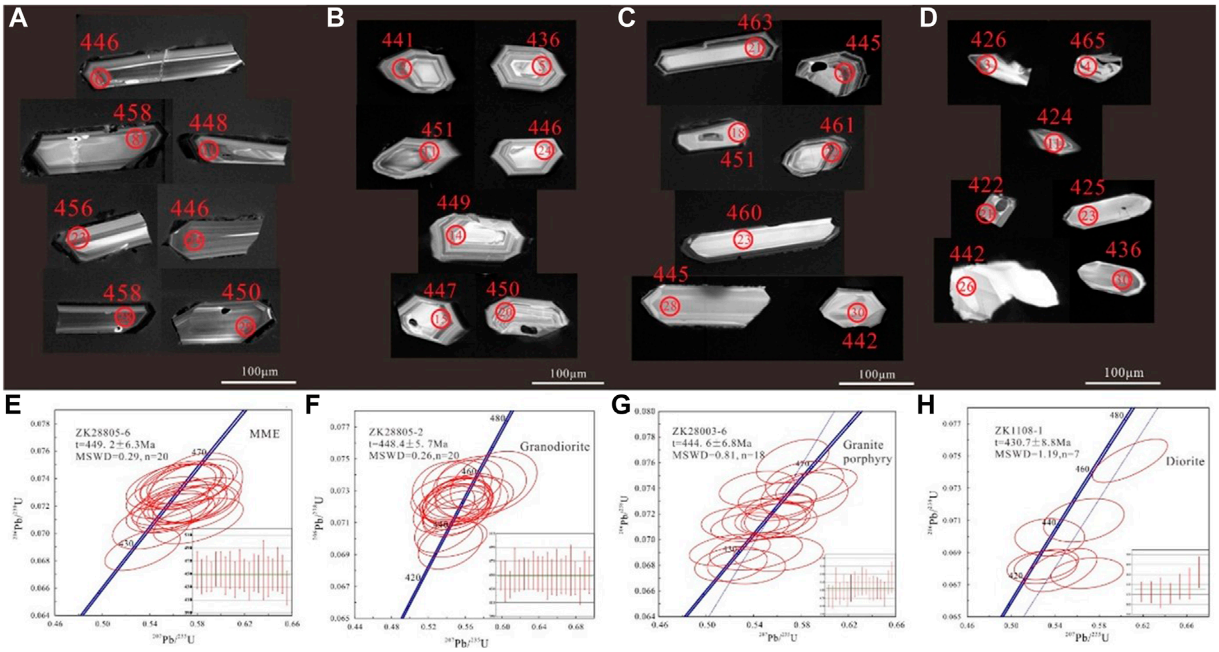

FIGURE 3
Cathodoluminescence (CL) images of zircon grains **(A–D)** and U–Pb concordia diagrams **(E–H)** for intrusive rocks in the Baoshan deposit. **(A, E)** ZK28805-6 MMEs, **(B, F)** ZK28805-2 granodiorites, **(C, G)** ZK28003-6 granite porphyries, (d and h) ZK1108-1 diorites.

melt and that these zircons are also typical magmatic zircons. After excluding discordant and inherited ages, 20 grains plot on or near a U–Pb concordia line, yielding a weighted mean $^{206}Pb/^{238}U$ age of 449.2 ± 6.3 Ma (MSWD = 0.29) (Figures 3A, E), which is interpreted to be the formation age of the MMEs. This age is in close proximity to the age of host granodiorites.

4.2 Whole-rock geochemistry

Geochemical data for granite porphyries, granodiorites, diorites and MMEs from the Baoshan deposit are listed in Table 1. In general, high field strength elements, rare earth elements and transition elements are stable during intense hydrothermal alteration, and Mg in intermediate–acidic igneous rock is also stable due to the lack of olivine and pyroxene. Ti, P, Al, Fe, Mn and other major elements are not easily affected by hydrothermal activity, while Ca, Na, K and some large ion lithophile elements (such as Sr, Ba, and Rb) are very unstable, and the obtained data may not accurately reflect the geochemical characteristics of rocks. Therefore, before interpreting the data, the impact of alteration should be fully considered to eliminate "distorted" data. All samples in this article have low LOI values (1.16%–2.18%), and there is no significant linear relationship between the contents of TiO_2, Al_2O_3, $Fe_2O_3^T$, MnO, MgO, CaO and LOI, suggesting slight effects of alteration on the studied samples. This is further supported by their subparallel REE and multi-element patterns (Figure 6).

After deducting the LOI, the granodiorites have moderate SiO_2 (65.12%–67.75%), Al_2O_3 (14.90%–16.00%), $Fe_2O_3^T$ (4.72%–5.63%), MgO (1.89%–2.37%), and CaO (4.34%–4.73%) contents. These rocks exhibit high $Mg^{\#}$ values (38.7–59.0) and relatively low alkali contents. On a SiO_2 vs $Na_2O + K_2O$ (TAS) diagram, data for the samples plot mainly in the quartz diorite and granodiorite fields (Figure 4A). When compared to the granodiorites, the granite porphyries have higher SiO_2 contents (75.21%) and lower $Fe_2O_3^T$ (1.20%), MgO (0.32%), and CaO (0.83%) contents, falling into the granite field (Figure 4A). When compared to the granodiorites and granite porphyries, the diorites havelower SiO_2 contents (59.06%) and higher $Fe_2O_3^T$ (8.01%), MgO (3.41%), and CaO (6.67%) contents. On a TAS diagram, data for the sample plot mainly in the diorite field (Figure 4A). On a SiO_2 vs K_2O diagram, the granite porphyries, granodiorites and diorites are classified as high-K calc-alkaline–shoshonite series, high-K calc-alkaline series and intermediate-K calc-alkaline series, respectively (Figure 4B). In an A/CNK vs A/NK diagram, the granodiorite and diorite samples plot mostly in the subalkaline–metaluminous field, whereas the granite porphyries plot in the weakly peraluminous field (Figure 4C). The MMEs have lower SiO_2 contents (53.69%–54.84%) and higher $Fe_2O_3^T$ (7.71%–10.56%), MgO (3.19%–6.52%), and CaO (5.40%–8.63%) contents than the host granodiorites. The MMEs plot in the monzodiorite–gabbrodiorite field on a TAS diagram and in the intermediate-to high-K calc-alkaline series on a SiO_2 vs K_2O diagram (Figures 4A, B). In an A/CNK vs A/NK diagram, data for the MMEs plot in the metaluminous to weakly peraluminous field (Figure 4C). In the Harker diagram, the correlations between TiO_2, Al_2O_3, $Fe_2O_3^T$, MnO, MgO, CaO, P_2O_5 and SiO_2 in the early Paleozoic intrusive rocks in the Baoshan deposit are negative, while the correlations between Na_2O and SiO_2 are positive (Figures 5A–H).

The total rare earth element (REE) contents of granite porphyries, granodiorites, diorites and MMEs from the Baoshan

 10.3389/feart.2024.1444751

TABLE 1 Major elements (wt%) and trace elements (ppm) analytical results for the intrusive rocks in the Baoshan deposit.

Intrusive Rocks	MMEs			Diorite	Granodiorite		Granite Porphyry
Sample No.	ZK28805-6	ZK1108-8	ZK28805-1	ZK1108-1	ZK28805-2	ZK28003-4	ZK28003-6
SiO_2	52.79	52.70	53.79	58.05	64.16	66.94	74.22
TiO_2	0.51	0.66	0.71	0.48	0.41	0.30	0.08
Al_2O_3	15.16	17.02	20.67	17.17	15.76	14.72	13.28
$Fe_2O_3{}^T$	10.38	9.74	7.56	7.87	5.55	4.66	1.18
MnO	0.42	0.19	0.10	0.16	0.12	0.13	0.04
MgO	6.41	5.35	3.13	3.35	2.33	1.87	0.32
CaO	6.67	8.47	5.30	6.56	4.66	4.29	0.82
Na_2O	3.66	2.23	4.09	3.19	2.69	2.82	3.44
K_2O	2.20	1.53	2.62	1.32	2.72	2.97	5.21
P_2O_5	0.13	0.20	0.12	0.14	0.12	0.10	0.09
LOI	1.61	2.18	1.22	1.95	1.30	1.16	1.24
Total	99.94	100.27	99.31	100.24	99.82	99.96	99.92
FeO_t	9.34	8.76	6.80	7.08	4.99	4.19	1.06
$Mg^\#$	59.0	56.1	49.1	49.8	49.5	48.3	38.7
Sc	47.5	30.0	19.6	17.8	15.6	11.7	4.40
V	319	406	156	201	147	113	17.0
Cr	160	90.0	140	20.0	30.0	30.0	10.0
Co	28.1	32.4	21.4	19.3	13.7	11.8	1.20
Ni	29.1	33.1	50.2	12.2	10.0	10.5	2.30
Cu	493	87.4	133	19.3	28.9	190	2.40
Zn	140	101	85.0	86.0	66.0	69.0	11.0
Ga	20.3	18.6	29.4	17.6	16.8	15.3	11.5
Rb	128	98.0	150	59.7	131	138	219
Sr	193	313	276	284	264	250	85.5
Y	53.2	26.8	25.0	18.3	22.4	16.2	20.1
Zr	102	64.0	112	122	142	117	64.0
Nb	15.8	8.00	15.9	5.90	10.2	7.60	6.90
Cs	7.36	4.34	9.44	3.30	8.53	7.80	8.01
Ba	392	340	793	452	743	592	507
La	17.6	19.3	61.9	18.7	18.2	20.4	14.1
Ce	45.6	42.1	116	37.4	36.2	38.3	26.3

(Continued on the following page)

TABLE 1 (*Continued*) Major elements (wt%) and trace elements (ppm) analytical results for the intrusive rocks in the Baoshan deposit.

Intrusive Rocks	MMEs			Diorite	Granodiorite		Granite Porphyry
Sample No.	ZK28805-6	ZK1108-8	ZK28805-1	ZK1108-1	ZK28805-2	ZK28003-4	ZK28003-6
Pr	6.53	5.49	13.1	4.29	4.29	4.13	2.80
Nd	28.2	21.4	46.7	15.8	16.3	14.6	9.60
Sm	7.00	4.42	8.26	3.06	3.40	2.65	2.11
Eu	1.42	1.03	1.35	0.83	0.78	0.64	0.44
Gd	7.40	4.41	6.62	3.03	3.37	2.55	2.35
Tb	1.25	0.70	0.91	0.47	0.55	0.40	0.43
Dy	8.69	4.66	5.17	3.14	3.67	2.65	3.18
Ho	1.85	0.97	0.94	0.66	0.77	0.57	0.68
Er	5.60	2.93	2.51	1.95	2.40	1.70	2.18
Tm	0.86	0.42	0.33	0.29	0.36	0.26	0.34
Yb	5.85	2.67	2.01	1.89	2.37	1.83	2.43
Lu	0.91	0.41	0.31	0.30	0.37	0.29	0.38
Hf	3.90	2.10	3.20	3.40	4.10	3.30	2.30
Ta	1.62	0.54	1.39	0.45	0.82	0.84	1.39
Th	11.1	6.86	23.1	9.66	15.2	19.0	15.0
U	6.17	1.46	5.33	2.11	3.88	5.04	9.83
ΣREE	138.8	110.9	265.6	91.81	93.03	90.97	67.32
Eu/Eu ∗	0.60	0.71	0.56	0.83	0.70	0.75	0.60
$(La/Yb)_N$	2.03	4.87	20.76	6.67	5.18	7.52	3.91
Rb/Sr	0.66	0.31	0.54	0.21	0.49	0.55	2.56
Nb/Ta	9.75	14.8	11.4	13.1	12.4	9.05	4.96
Rb/Nb	8.07	12.25	9.43	10.12	12.8	18.1	31.7

Note: $Eu/Eu^* = Eu_N/(Sm_N \times Gd_N)^{0.5}$.
where N represents normalization value after (Sun and McDonough, 1989). "t" means "in total", assuming that total Fe in rocks appear as Fe_2O_3.

deposit show a gradually increasing trend (265.6–67.32 ppm). The granite porphyries have a relatively flat REE pattern, with moderate negative Eu anomalies (0.60) and no prominent light to heavy REE fractionation ($(La/Yb)_N$ = 3.9; N represents the chondrite-normalised value). The diorite and granodiorites have similar REE patterns, showing light REE enrichment ($(La/Yb)_N$ = 6.7 and 5.2–7.5), with small negative Eu anomalies (0.83 and 0.70–0.75). Most MMEs have relatively flat REE patterns, with moderate negative Eu anomalies (0.60–0.71) and no prominent light to heavy REE fractionation ($(La/Yb)_N$ = 2.0–4.9). Other MMEs have listric-shaped LREE enrichment patterns, with moderate negative Eu anomaly (0.56) and prominent light to heavy REE fractionation ($(La/Yb)_N$ = 20.8) (Figure 6A). In primitive mantle-normalized trace element patterns, many MMEs show characteristics similar to both the granodiorites and diorites, exhibiting enrichment of large-ion lithophile elements (e.g., Rb and K) and depletion of high-field-strength elements (e.g., Nb, Ta, and Ti). However, other MMEs have similar patterns to those of the granite porphyries, exhibiting no negative Ta anomalies (Figure 6B).

The Sc, Cr, Ni, V, and Co concentrations of the MMEs are the highest, followed by the granodiorites and diorites, and those of the granite porphyries are the lowest. Rb/Nb ratios of the granite porphyries, granodiorites, diorites and MMEs (31.74, 12.79–18.09, 10.12, and 8.07–12.25) are higher than that of mantle-derived

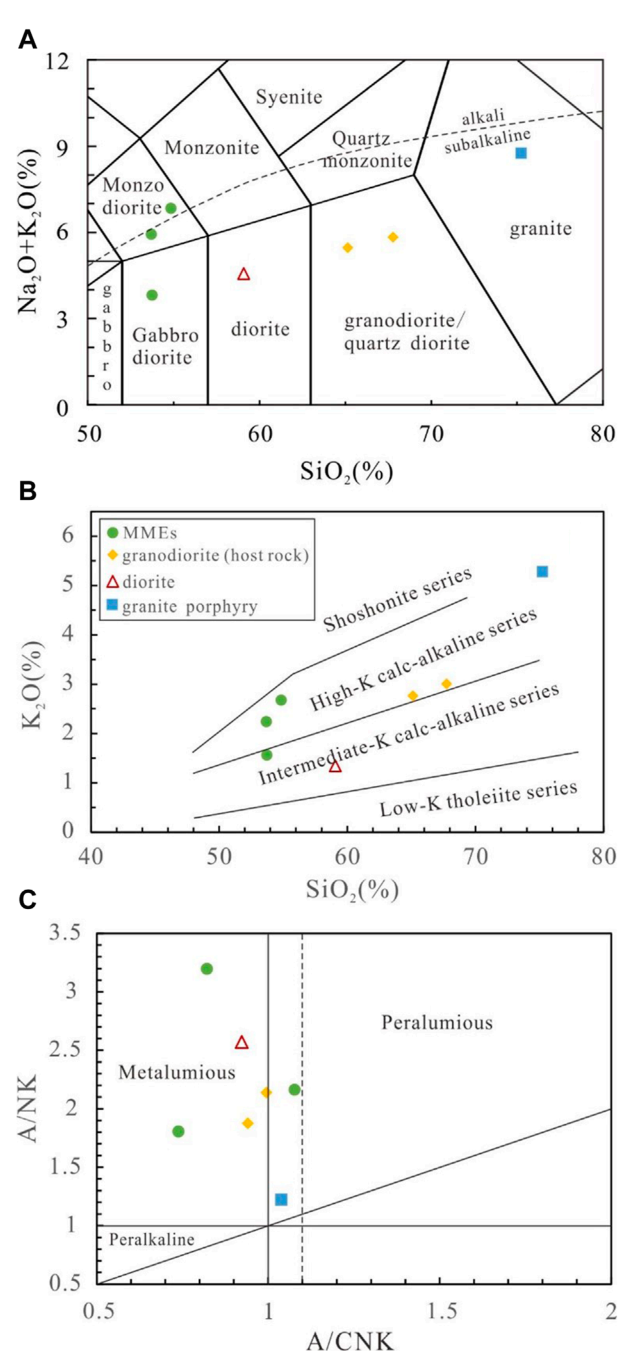

FIGURE 4
Geochemical discrimination diagrams for intrusive rocks in the Baoshan deposit. **(A)** TAS diagram after Wilson (1989); **(B)** SiO_2 *versus* K_2O diagram after Peccerillo and Taylor (1976); **(C)** A/CNK *versus* A/NK diagram after Middlemost (1985) and Maniar and Piccoli (1989), where A/NK = Al_2O_3 (molar)/(Na_2O + K_2O) (molar) and A/CNK = Al_2O_3 (molar)/(K_2O + Na_2O + CaO) (molar).

magmatic granite (0.05), while the Rb/Sr ratio of granite porphyries (2.56) is higher than that of crust-derived magmatic granite (0.5) (Sylvester, 1998). The Nb/Ta ratios of the granodiorites, diorites and MMEs (9.05–12.44, 13.11, and 9.75–14.81, respectively) are intermediate between the continental crust (8.30) and primitive mantle (17.50), while the Nb/Ta ratio of the granite porphyries (4.96) are lower than the value for continental crust (Sun and McDonough, 1989). The $Mg^{\#}$ value of granodiorites, diorites and MMEs (48.33–49.45, 49.80, and 49.11–59.00, respectively) are higher than the value of crust-derived granite (<40) (Atherton and Petford, 1993), while the $Mg^{\#}$ value of granite porphyries (38.7) are lower than the value of crust-derived granite.

4.3 Hf isotopes

The samples have low zircon $^{176}Lu/^{177}Hf$ ratios (less than 0.002), indicating little accumulation of radiogenic Hf after zircon formation (Wu et al., 2007a). The zircon εHf(t) values of the granite porphyries, granodiorites, diorites and MMEs range from −3.2 to −0.3, from −2.9 to −0.6, from −5.5 to +3.1, and from −2.3 to +0.6, respectively (Figure 7A). Such variations are much larger than analytical uncertainties, indicating that these samples have heterogeneous zircon Hf isotopic compositions. Correspondingly, the two-stage Hf isotope model ages of the samples primarily range from 1.1 Ga to 1.6 Ga (Figure 7B, Supplementary Table S2).

5 Discussion

5.1 I-type granitoids in the Baoshan deposit

According to the magma source and tectonic setting, the granites can be divided into four types: M-, A-, S-, and I-type granites (Whalen et al., 1987; Chappell, 1999). M-type granite, also known as mantle-derived granite, is formed by fractional crystallization from a tholeiitic magma series (Wu et al., 2007b). The granite porphyries, granodiorites and their MMEs are part of the calc-alkaline magma series (Figures 4A, B), and most of zircon $\varepsilon_{Hf}(t)$ values are negative (Figure 7), indicating that they are mainly derived from crust rather than mantle. The zircon Ti temperatures of granite porphyries, granodiorites and their MMEs are of 671°C–775°C (av. of 726 C), 683°C–751°C (av. of 716°C) and 648°C–708°C (av. of 679°C), indicating a low formation temperature (Ferry and Watson, 2007). This is not consistent with the A-type granite formed in a high-temperature and low-pressure environment. The typical A-type granites have important mineralogical and geochemical signatures, such as alkaline dark minerals, high 10,000×Ga/Al (>2.6), and high Zr + Nb + Ce + Y (>350 ppm) (Whalen et al., 1987). The granodiorites and granite porphyries have low 10,000×Ga/Al (1.6–2.0) ratios and low Zr + Nb + Ce + Y (117–211 ppm) contents without any alkaline dark minerals found under the microscope, further supporting that the granodiorites and granite porphyries are not A-type granites (Figures 8A, B).

S-type granite is mainly a product of partial melting of crustal sedimentary rocks. The typical S-type granite is strongly peraluminous, and show an A/CNK value (>1.1) and a significant Eu anomaly (Miller, 1985). The A/CNK values (0.74–1.08) of granite porphyries, granodiorites and their MMEs are less than 1.1, which plot in the metaluminous to weakly peraluminous area (Figure 4C). Their Eu anomalies are not obvious (0.60–0.83), indicating that the granite porphyries, granodiorites and their MMEs are not S-type granitoids. I-type granite is mainly the product of partial

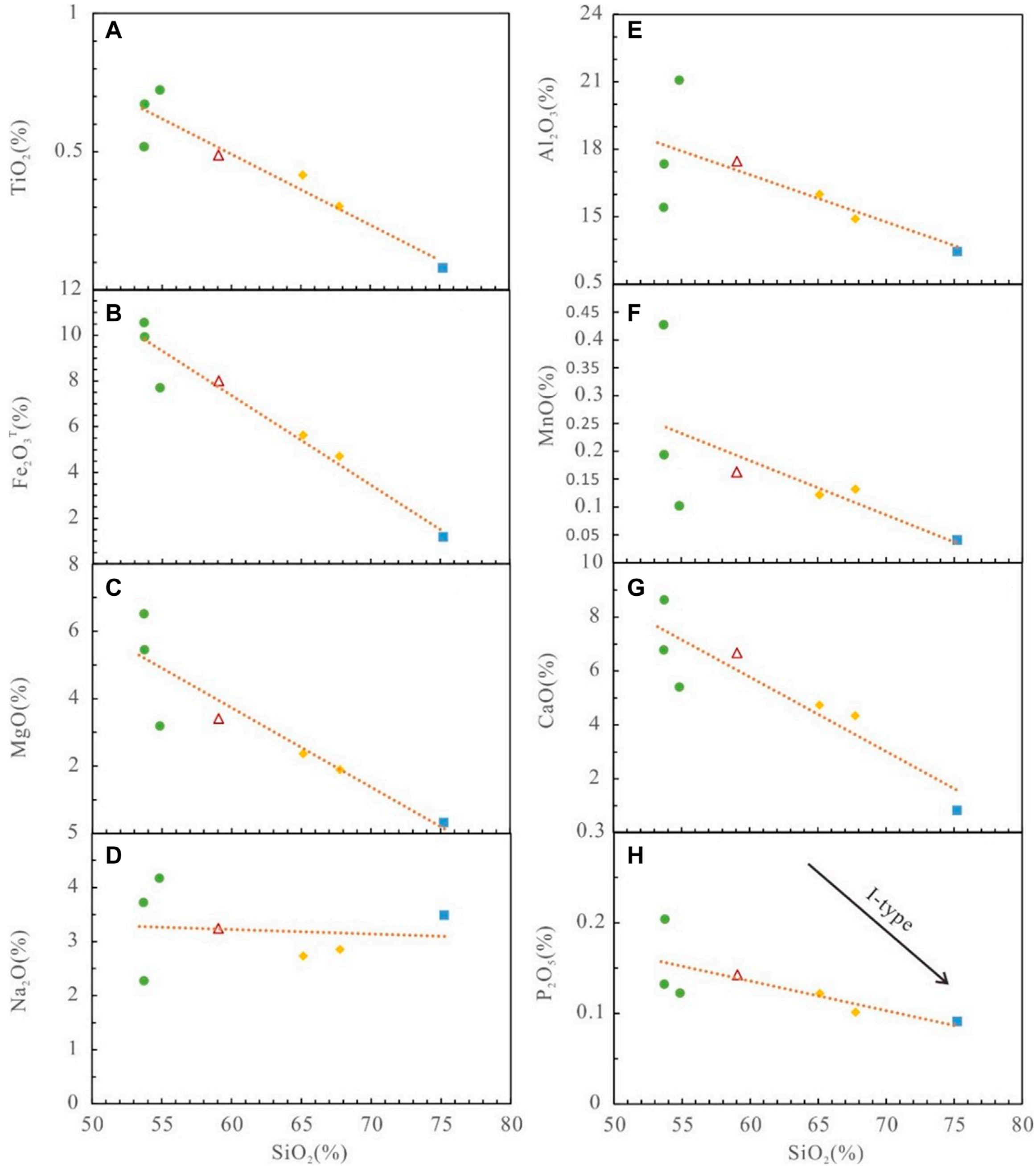

FIGURE 5
(A–H) Harker diagrams for intrusive rocks in the Baoshan deposit. Symbols are the same as in Figure 4B.

melting of crustal igneous rocks. The characteristic minerals of I-type granite are hornblende and pyroxene, with an A/CNK value less than 1.1. Components like biotite and hornblende are commonly found in the granite porphyries, granodiorites and their MMEs (Figure 2), showing an I-type granite affinity (Chappell and White, 1974). On the diagrams of FeO_t/MgO–Zr + Nb + Ce + Y and 10,000×Ga/Al–Zr + Nb + Ce + Y (Figures 8A, B), granite porphyries and granodiorites are situated within the undifferentiated I-, S-, and M-type granitoids. On the SiO_2 *versus* P_2O_5 diagram (Figure 5H), the samples show evolutionary trends typical of I-type granitoids (Wang et al., 2022). The samples in this study contain hornblende (Figure 2). Thus, the granite porphyries, granodiorites and its associated MMEs from the Baoshan deposit belong to I-type granitoids.

5.2 Petrogenesis of the intrusive rocks and mantle-derived contribution

The genesis of calc-alkaline I-type granites has been attributed to the following mechanisms: 1) partial melting of residual basaltic oceanic crust and sediment (Castro et al., 2010; Huang et al., 2014; Zhang Y. et al., 2016; Shao et al., 2017); 2) assimilation–fractional crystallization and contamination (AFC) of mantle–derived basaltic

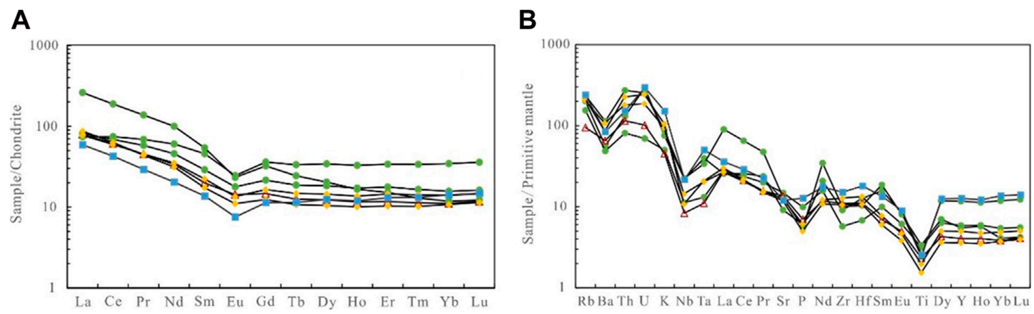

FIGURE 6
Chondrite-normalized REE **(A)** and primitive-mantle-normalized trace element patterns **(B)** for intrusive rocks in the Baoshan deposit. Normalizing values for chondrite and primitive mantle are from Sun and McDonough (1989). Symbols are the same as in Figure 4B.

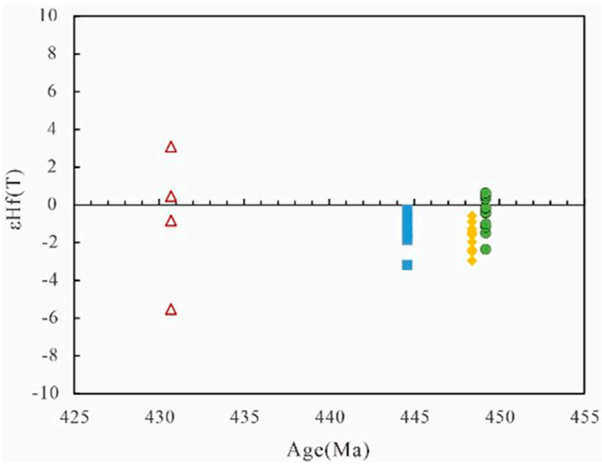

FIGURE 7
Age *versus* εHf (t) diagram of zircons in intrusive rocks in the Baoshan deposit (Nowell et al., 1998; Vervoort and Blichert-Toft, 1999). Symbols are the same as in Figure 4B.

magma (Chen and Arakawa, 2005; Souza et al., 2007); 3) partial melting of deep or shallow crustal materials (Laurent et al., 2014; Liu et al., 2015); and 4) magma mixing of crust- and mantle-derived magmas (Dong et al., 2011; Xie et al., 2020; Tang et al., 2021).

For granitic rocks, if the Hf isotope model age is similar to its formation age, then its source is juvenile crust (Ferry and Watson, 2007). The zircon ε_{Hf}(t) values of granite porphyries, diorites, granodiorites and MMEs (~450–430 Ma) mainly range from −5.5 to + 3.1, and the corresponding T_{DM2} ages range from 1.1 Ga to 1.6 Ga, indicating that the intrusive rocks in the Baoshan deposit mainly originated from partial melting of Mesoproterozoic crust. In addition, the zircon $(^{176}Hf/^{177}Hf)_i$ values (0.28182–0.28258) are lower than those of chondrites (0.28277), also indicating that their diagenetic materials mainly originated from the crust.

The granite porphyry samples fall in the field of the partial melt of metagreywacke or metapelite (Figures 9A, C), whereas the diorites, granodiorites, and their MMEs are plotted in the partial melt extending from metabasalt to metatonalite (Figures 9A, C). This distinction suggests that granite porphyries and other rocks may have undergone partial melting in varying source materials. They exhibit lower Al_2O_3/TiO_2, Rb/Sr and Rb/Ba ratios but higher CaO/Na_2O ratio compared to the typical metapelite derived melt (Figures 9B, D). Such signatures indicate variations in the compositions and origins of these rocks, and such compositions could not solely originate from crustal-derived sources. Instead, an evident transitional trend between pelite and basalt-derived melts reveals the input of mantle-derived materials cannot be precluded in the genesis of the I-type granites.

The samples show an obvious magmatic mingling trend in the MgO-FeO^T diagram (Figure 10A). The minerals in MMEs are euhedral–subhedral and much smaller than those in the host granodiorites (Figure 2). The zircon Eu anomalies of MMEs are much weaker than those of the host granodiorites. MMEs and their host granodiorites have a clear boundary and present a dark grey condensation edge (Figure 2F), further indicating that they formed through the mixing of magmas derived from different sources (Nitoi et al., 2002; Perugini et al., 2003). In contrast, there is no obvious fractional crystallization trend in the Sr-Eu/Eu∗, 10,000∗Ga/Al-Rb/Sr and Rb-Ba diagrams, indicating that fractional crystallization had little effect on magma genesis (Figures 10B–D). In addition, the zircon εHf(t) values of the samples show a large variation (2–24 ε units), and the range of the $(^{176}Hf/^{177}Hf)_i$ values is also relatively large. Considering that zircon Hf isotopes cannot be altered by fractional crystallization or partial melting, such zircon Hf isotope variations have been interpreted to result from magma mingling between mantle- and crust-derived magmas (Bolhar et al., 2008; Zhu et al., 2009; Ji et al., 2018).

5.3 Implications for Early Paleozoic geodynamic evolution in the SCB

The Early Paleozoic tectonic setting of the SCB remains enigmatic. Although more and more scholars prefer an intra-continental orogeny rather than a subduction-collisional orogeny (Chen and Huang, 2012; Cawood et al., 2013; Li, 2013; Zhang et al., 2015; Zhang X. S. et al., 2016; Qin et al., 2017; Wang et al., 2018; Shu et al., 2020; Gan et al., 2023), there is still a divergence between intra-continental homo-collision and post-collision extension (Shu et al., 2008; Faure et al., 2009; Zhang et al., 2009; Jia et al., 2022). In recent years, with the study of MMEs (Nong et al.,

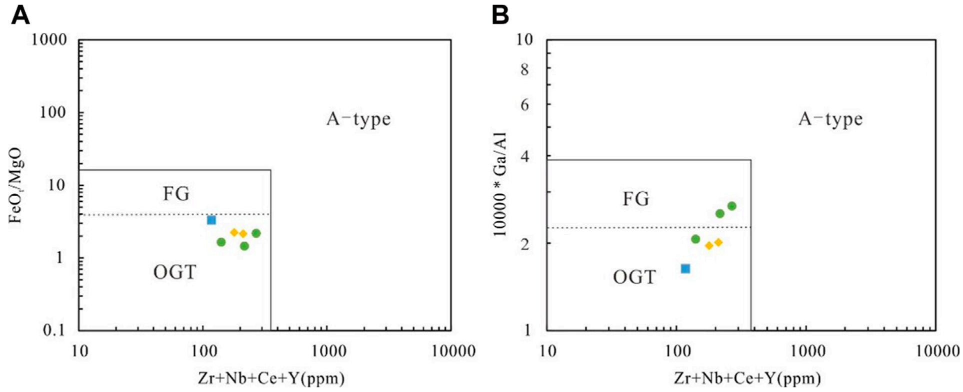

FIGURE 8
(A) Zr + Nb + Ce + Y *versus* FeO_t/MgO and **(B)** Zr + Nb + Ce + Y *versus* 10,000 ∗ Ga/Al (Whalen et al., 1987) diagrams for intrusive rocks in the Baoshan deposit. OGT—field for I-, S-, and M-type granitoids; FG—field for fractionated I-type granitoids. Symbols are the same as in Figure 4B.

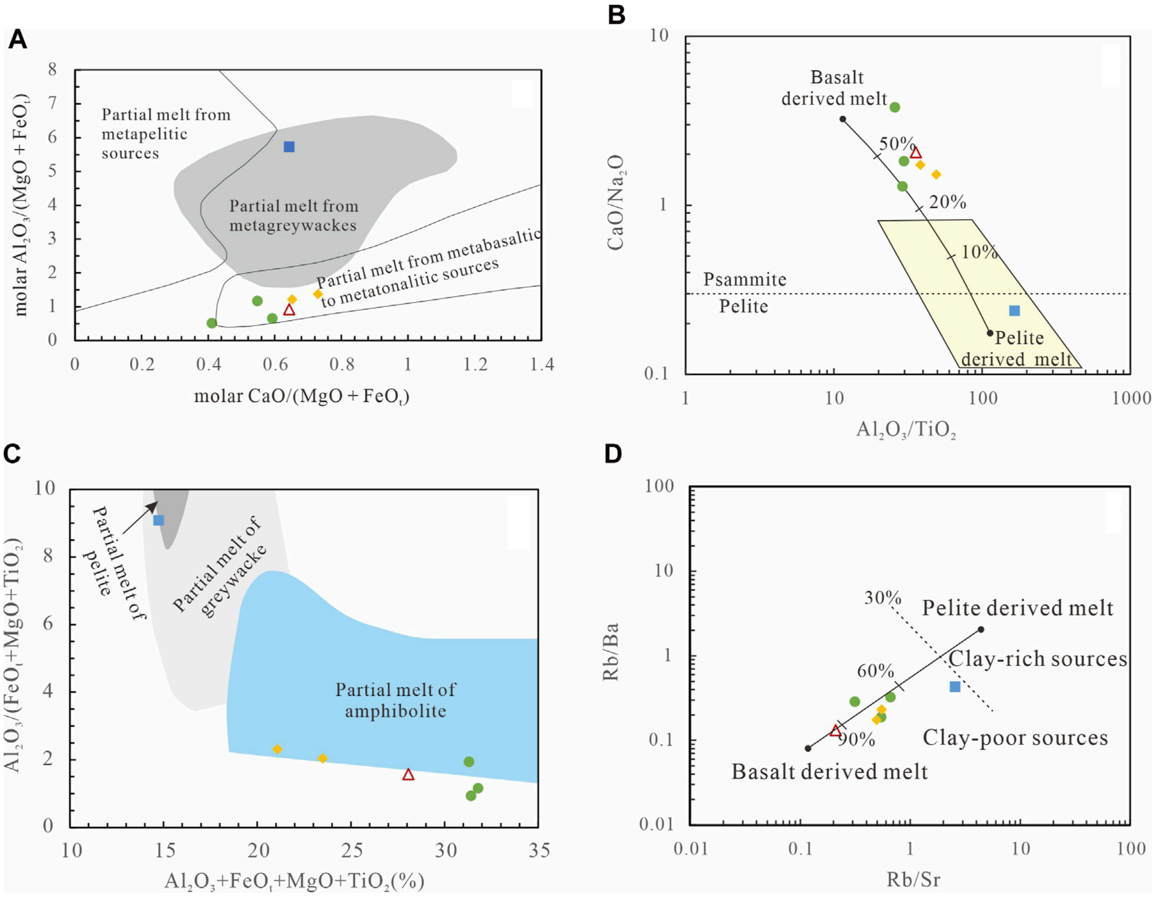

FIGURE 9
Source discrimination diagrams for intrusive rocks in the Baoshan deposit: **(A)** molar $CaO/(MgO + FeO_t)$ *versus* molar $Al_2O_3/(MgO + FeO_t)$ after (Altherr and Siebel, 2002); **(B)** Al_2O_3/TiO_2 *versus* CaO/Na_2O, **(C)** (Al_2O_3 + FeO_t + MgO + TiO_2) *versus* $Al_2O_3/(FeO_t + MgO + TiO_2)$, **(D)** Rb/Sr *versus* Rb/Ba after (Sylvester, 1998). Symbols are the same as in Figure 4B.

2017a) and mafic rocks (Nong et al., 2017b) in the Dayaoshan region, it is confirmed that the tectonic environment of this area may have been collision to extension transition during the Early Paleozoic. In addition, the existence of Early Paleozoic high-Mg basalts in northern Guangdong Province (ca. 442–435 Ma) (Wang et al., 2013), the lamprophyre found near the Daning pluton in northeastern Guangxi (ca. 440 Ma) (Yao et al., 2012; Jia et al., 2017), and the dacites found in northern Guangdong Province (ca. 450 Ma) (Yi et al., 2014) indicates that the transition from collision to extension was likely postponed to at least 450–435 Ma.

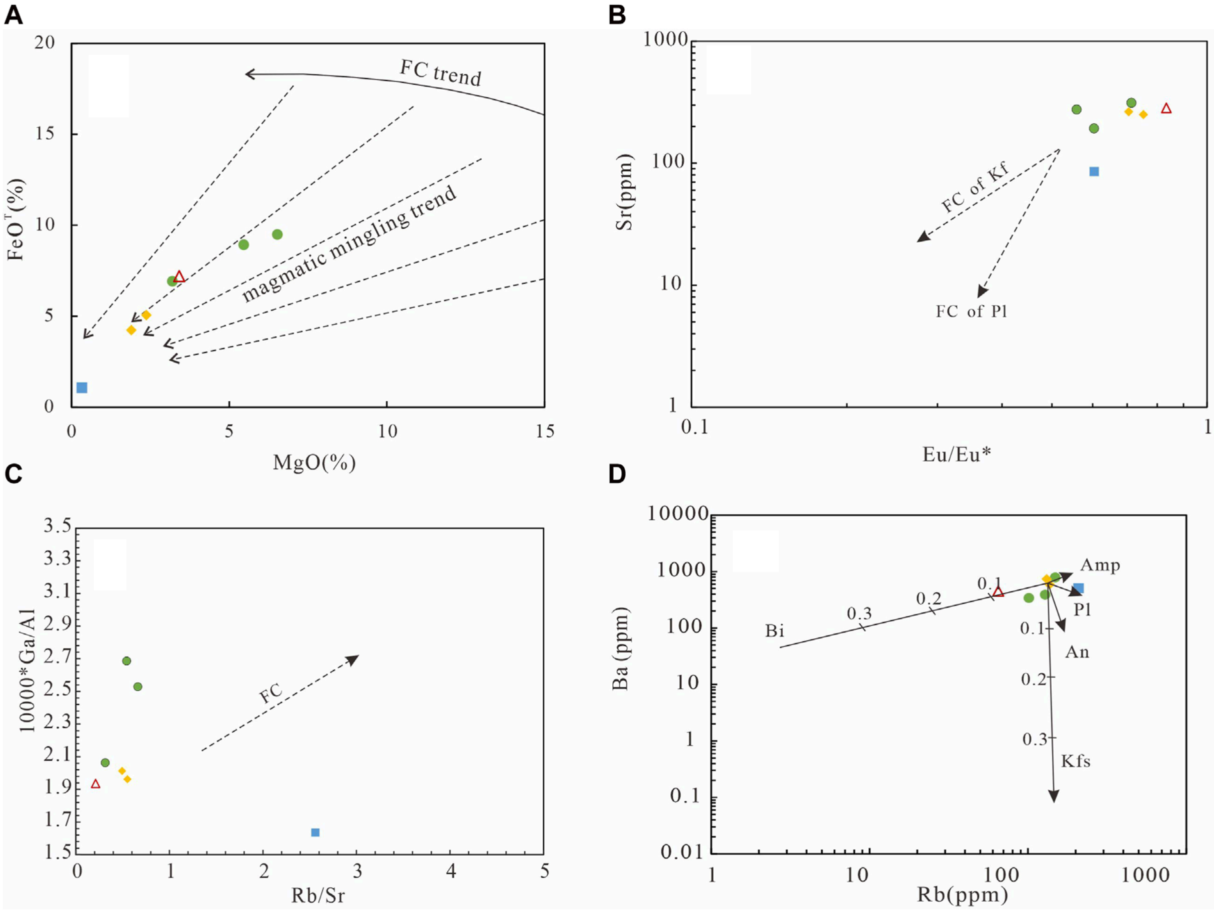

FIGURE 10
Geochemical classification diagrams for intrusive rocks in the Baoshan deposit. **(A)** MgO *versus* FeO^T after (Zorpi et al., 1989); **(B)** Eu/Eu ∗ *versus* Sr; **(C)** Rb/Sr *versus* 10,000 ∗ Ga/Al; **(D)** Rb *versus* Ba after (Hanson and Sun, 1976; Ewart and Griffin, 1994). Symbols are the same as in Figure 4B.

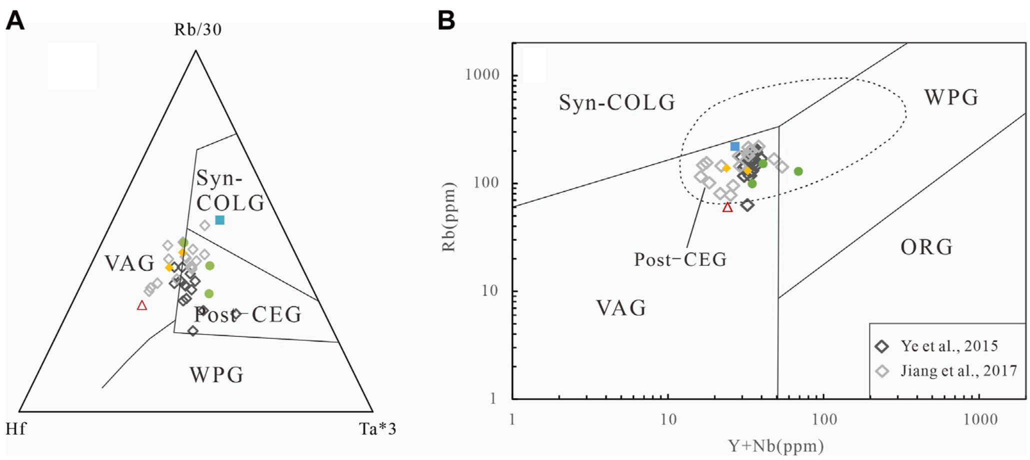

FIGURE 11
Diagrams of **(A)** Rb/30-Hf-Ta ∗ 3 and **(B)** Rb *versus* Y + Nb for intrusive rocks in the Baoshan deposit. The tectono-magmatic discrimination diagrams for granitoids are from Pearce et al. (1984); Forster et al. (1997); Harris et al. (1986). VAG-volcanic arc granites; WPG-within-plate granites; syn-COLG, syn-collisional granites; ORG-ocean ridge granites; post-CEG, post-collisional extensional granites. Symbols are the same as in Figure 4B.

The granite porphyries, diorites, granodiorites and their MMEs in the Baoshan deposit were formed at 450–430 Ma. Therefore, these rocks in the study area were formed in the local extension-thinning environment of the lithosphere following the intra-continental collision orogeny.

The geochemical characteristics of the diorites, granodiorites, and their MMEs are similar to those in the Daning, Gulong, and Dacun plutons of northeastern Guangxi (438–435 Ma) (Li et al., 2006; Nong et al., 2017a; Liu et al., 2020) and the Longxin, Liandong, and Xiaying plutons of southeastern Guangxi (447–434 Ma) (Liu et al., 2021; Zhou et al., 2023), indicating a crust–mantle mixing origin. These previous studies also confirmed that mingling of magmas derived from the crust and mantle played an important role in the formation of Early Paleozoic granitoids in the SCB. These I-type granitoids with these petrogenetic characteristics are consistent with an origin in an extensional setting. On tectonic discrimination diagrams (Figure 11), our studied samples and previously-published data plot within the volcanic arc granites and the post-collisional extensional granites field. The zircon Hf isotope results indicate that the mantle components are indeed involved in the formation of granites, and underplating may be a geological process that is closely related to the genesis of granite (Petford and Gallagher, 2001; Annen and Sparks, 2002). Based on this result, combined with the above discussion, we propose that the granite porphyries, diorites, granodiorites and its MMEs in the Baoshan deposit were probably produced by the remelting of Mesoproterozoic crust as a result of underplating of mantle-derived magma, and magma mingling occurred during the tectonic transition from collision to extension in the Early Paleozoic. The mantle-derived magmas played an important role in the formation of the Early Paleozoic intrusive rocks and MMEs via their heat and material input.

6 Conclusion

(1) The granodiorites and its associated MMEs, granite porphyries, and diorites from the Baoshan deposit show zircon U-Pb ages of 448.4 ± 5.7 Ma, 449.2 ± 6.3 Ma, 444.6 ± 6.8 Ma, and 430.7 ± 8.8 Ma, respectively.

(2) The granite porphyries, granodiorites and their MMEs belong to metaluminous to weakly peraluminous calc-alkaline I-type granitoids.

(3) The granite porphyries, diorites, granodiorites, and their associated MMEs were mainly derived from partial melting of Mesoproterozoic crust with the input of few mantle-derived materials, in response to a transition from a collisional tectonic setting to an extensional environment.

Data availability statement

The original contributions presented in the study are included in the article/Supplementary Material, further inquiries can be directed to the corresponding author.

Author contributions

PL: Data curation, Formal Analysis, Investigation, Visualization, Writing–original draft, Writing–review and editing. FL: Writing–review and editing, Data curation, Formal Analysis, Investigation, Visualization. LC: Writing–review and editing, Formal Analysis, Visualization. ZS: Writing–review and editing, Data curation, Formal Analysis. WM: Writing–review and editing, Investigation. YH: Writing–review and editing, Investigation.

Funding

The author(s) declare that financial support was received for the research, authorship, and/or publication of this article. This research was funded by Specific Research Project of Guangxi for Research Bases and Talents (AD20159026; AD22035046), Guangxi Bagui Scholars Special Fund, and the Natural Science Foundation of Fujian Province (Grant No. 2021J05229).

Acknowledgments

We are grateful for the generous support of Guangxi Zhuang Autonomous Region Geophysical Survey Institute in field investigations and formal analyses. We sincerely thank Jiangbo Ren and Yunfeng Wang for their inspirational discussion. We would like to thank the editors and the reviewers for their constructive comments and suggestions.

Conflict of interest

The authors declare that the research was conducted in the absence of any commercial or financial relationships that could be construed as a potential conflict of interest.

Publisher's note

Supplementary material

The Supplementary Material for this article can be found online at: https://www.frontiersin.org/articles/10.3389/feart.2024.1444751/full#supplementary-material

References

Altherr, R., and Siebel, W. (2002). I-type plutonism in a continental back-arc setting: miocene granitoids and monzonites from the central Aegean Sea, Greece. *Contrib. Mineral. Petrol.* 143 (4), 397–415. doi:10.1007/s00410-002-0352-y

Annen, C., and Sparks, R. S. J. (2002). Effects of repetitive emplacement of basaltic intrusions on thermal evolution and melt generation in the crust. *Earth Planet Sci. Lett.* 203 (3-4), 937–955. doi:10.1016/s0012-821x(02)00929-9

Atherton, M. P., and Petford, N. (1993). Generation of sodium-rich magmas from newly underplated basaltic crust. *Nature* 362 (6416), 144–146. doi:10.1038/362144a0

Barbarin, B. (2005). Mafic magmatic enclaves and mafic rocks associated with some granitoids of the central Sierra Nevada batholith, California, Nature, origin, and relations with the hosts. *Lithos* 80 (1), 155–177. doi:10.1016/j.lithos.2004.05.010

Bi, S. J., Yang, Z., Li, W., Liang, P., and Tang, K. F. (2015). Discovery of late Cretaceous Baoshan porphyry copper deposit in Dayaoshan, Qinhang metallogenic belt, Constraints from zircon U-Pb age and Hf isotope. *Earth Sci. J. China Univ. Geosci.* 40 (9), 1458–1479. doi:10.3799/dqkx.2015.132

Bolhar, R., Weaver, S. D., Whitehouse, M. J., Palin, J. M., Woodhead, J. D., and Cole, J. W. (2008). Sources and evolution of arc magmas inferred from coupled O and Hf isotope systematics of plutonic zircons from the Cretaceous Separation Point Suite (New Zealand). *Earth Planet Sci. Lett.* 268 (3–4), 312–324. doi:10.1016/j.epsl.2008.01.022

Castro, A., Gerya, T., García-casco, A., Fernández, C., Díaz-Alvarado, J., Moreno-Ventas, I., et al. (2010). Melting relations of MORB–sediment mélanges in underplated mantle wedge plumes, Implications for the origin of Cordilleran-type batholiths. *J. Petrology* 51 (6), 1267–1295. doi:10.1093/petrology/egq019

Cawood, P. A., Wang, Y. J., Xu, Y. J., and Zhao, G. C. (2013). Locating South China in Rodinia and Gondwana, A fragment of greater India lithosphere? *Geology* 41 (8), 903–906. doi:10.1130/g34395.1

Chappell, B. W. (1999). Aluminium saturation in I- and S-type granites and the characterization of fractionated haplogranites. *Lithos* 46 (3), 535–551. doi:10.1016/s0024-4937(98)00086-3

Chappell, B. W., and White, A. J. R. (1974). Two contrasting granite types. *Pac. Geol.* 8, 173–174.

Chen, B., and Arakawa, Y. (2005). Elemental and Nd-Sr isotopic geochemistry of granitoids from the West Junggar fold belt (NW China), with implications for Phanerozoic continental growth. *Geochimica Cosmochimica Acta* 69 (5), 1307–1320. doi:10.1016/j.gca.2004.09.019

Chen, L., Pan, L., Huang, F., and Xu, J. F. (2018). Magma mixing in the giant Pulang porphyry copper deposit, Yunnan province, evidence from melt inclusions. *Geotect. Metallogenia* 42 (5), 880–892. doi:10.16539/j.ddgzyckx.2018.05.006

Chen, M. H., and Huang, Z. Z. (2012). Geochemistry of granitoid rocks of Shedong W-Mo deposit district in Cangwu County, Guangxi and its relation to mineralization. *Acta Petrol. Sin.* 28 (1), 199–212.

Chen, M. H., Li, Z. Y., and Li, Q. (2015). A preliminary study of multi-stage granitoids and related metallogenic series in Dayaoshan area of Guangxi, China. *Earth Sci. Front.* 22 (2), 41–53. doi:10.13745/j.esf.2015.02.004

Chen, M. H., Mo, C. S., Huang, Z. Z., Li, B., and Huang, H. W. (2011). Zircon LA-ICP-MS U-Pb ages of granitoid rocks and molybdenite Re-Os age of Shedong W-Mo deposit in Cangwu County of Guangxi and its geological significance. *Min. Depos.* 30 (6), 963–978. doi:10.16111/j.0258-7106.2011.06.001

Cheng, S. B., Fu, J. M., Xu, D. M., Ma, L. Y., Pang, Y. C., and Cao, L. (2009). Geochemical characteristics and petrogenesis of Xuehuading granitic batholith and its enclaves, South China. *Geotect. Metallogenia* 33 (4), 588–597. doi:10.16539/j.ddgzyckx.2009.04.010

Didier, J., and Barbarin, B. (1991). Enclaves and granite petrology. *Amst. Elsevier* 13, 1–625.

Dong, Y. P., Zhang, G. W., Neubauer, F., Liu, X. M., Hauzenberger, C., Zhou, D. W., et al. (2011). Syn- and post-collisional granitoids in the Central Tianshan orogen: geochemistry, geochronology and implications for tectonic evolution. *Gondwana Res.* 20 (2), 568–581. doi:10.1016/j.gr.2011.01.013

Ewart, G. W. L., and Griffin, W. (1994). Application of proton-microprobe data to trace-element partitioning in volcanic rocks. *Chem. Geol.* 117 (1-4), 251–284. doi:10.1016/0009-2541(94)90131-7

Faure, M., Shu, L. S., Wang, B., Charvet, J., Choulet, F., and Monie, P. (2009). Intracontinental subduction: a possible mechanism for the early palaeozoic orogen of SE China. *Terra nova.* 21 (5), 360–368. doi:10.1111/j.1365-3121.2009.00888.x

Ferry, J. M., and Watson, E. B. (2007). New thermodynamic models and revised calibrations for the Ti-in-zircon and Zr-in-rutile thermometers. *Contrib. Mineral. Petrol.* 154 (4), 429–437. doi:10.1007/s00410-007-0201-0

Forster, H. J., Tischendorf, G., and Trumbull, R. B. (1997). An evaluation of the Rb vs. (Y + Nb) discrimination diagram to infer tectonic setting of silicic igneous rocks. *Lithos* 40 (2-4), 261–293. doi:10.1016/s0024-4937(97)00032-7

Gan, C. S., Qian, X., Zhang, Y. Z., Bai, T. X., and Wang, Y. J. (2023). Provenance variation of the Cambrian-Ordovician sedimentary rocks across South China and implication for its paleogeography in East Gondwana. *Lithos* 454-455, 107242. doi:10.1016/j.lithos.2023.107242

Guan, Y. L., Yuan, C., Long, X. P., Zhang, Y. Y., Wang, X. Y., Huang, Z. Y., et al. (2016). Genesis of mafic enclaves from early Paleozoic granites in the south China block, evidence from petrology, geochemistry and zircon U-Pb geochronology. *Geotect. Metallogenia* 40 (1), 109–124. doi:10.16539/j.ddgzyckx.2016.01.010

Guo, C. L., and Liu, Z. K. (2021). Caledonian granites in south China: the geological and geochemical characteristics on their petrogenesis and mineralization. *J. Earth Sci. Environ.* 043 (006), 927–961. doi:10.19814/j.jese.2021.07026

Hanson, G. N., and Sun, S. S. (1976). Rare earth element evidence for differentiation of McMurdo volcanics, Ross Island, Antarctica. *Contrib. Min. Petrol.* 54, 139–155. doi:10.1007/bf00372120

Harris, N. B. W., Pearce, J. A., and Tindle, A. G. (1986). Geochemical characteristics of collision-zone magmatism. In: M. P. Coward, and A. C. Ries Editors, *Geochemical characteristics of collision-zone magmatism*, (London, Special Publications). 19 (1), 67–81. doi:10.1144/gsl.sp.1986.019.01.04

Hawkesworth, C. J., and Kemp, A. I. S. (2006). Using hafnium and oxygen isotopes in zircons to unravel the record of crustal evolution. *Chem. Geol.* 226 (3-4), 144–162. doi:10.1016/j.chemgeo.2005.09.018

Hoskin, P. W. O., and Schaltegger, U. (2003). The composition of zircon and igneous and metamorphic petrogenesis. *Mineralogy Geochem.* 53 (1), 27–62. doi:10.2113/0530027

Hu, S. Q., Zhou, G. f., Peng, S. B., Zhang, X. J., Yi, S. H., and Tang, G. S. (2012). Chronology and geochemical characteristics of quartz monzonite (porphyry) in the Dali copper-molybdenum deposit and its geological significance. *Acta Geosci. Sin.* 33 (1), 23–37.

Huang, D. L., and Wang, X. L. (2019). Reviews of geochronology, geochemistry and geodynamic processes of Ordovician-Devonian granitic rocks in Southeast China. *J. Asian Earth Sci.* 184, 104001. doi:10.1016/j.jseaes.2019.104001

Huang, H., Niu, Y. L., Nowell, G. M., Zhao, Z. D., Yu, X., Zhu, D. C., et al. (2014). Geochemical constraints on the petrogenesis of granitoids in the East Kunlun Orogenic belt, northern Tibetan Plateau: implications for continental crust growth through syn-collisional felsic magmatism. *Chem. Geol.* 370, 1–18. doi:10.1016/j.chemgeo.2014.01.010

Huang, W. T., Liang, H. Y., Zhang, J., Wu, J., Chen, X. L., and Ren, L. (2019). Genesis of the Dachang Sn-polymetallic and Baoshan Cu ore deposits, and formation of a Cretaceous Sn-Cu ore belt from southwest China to western Myanmar. *Ore Geol. Rev.* 112, 103030. doi:10.1016/j.oregeorev.2019.103030

Jackson, S. E., Pearson, N. J., Griffin, W. L., and Belousova, E. A. (2004). The application of laser ablation-inductively coupled plasma-mass spectrometry to *in situ* U-Pb zircon geochronology. *Chem. Geol.* 211 (1-2), 47–69. doi:10.1016/j.chemgeo.2004.06.017

Janoušek, V., Braithwaite, C. J. R., Bowes, D., and Gerdes, A. (2004). Magma-mixing in the genesis of Hercynian calc-alkaline granitoids, an integrated petrographic and geochemical study of the Sázava intrusion, Central Bohemian Pluton, Czech Republic. *Lithos* 78 (1), 67–99. doi:10.1016/j.lithos.2004.04.046

Ji, X. F., Wei, Q. R., Li, S. J., Xu, H., Wang, X. D., Chen, T. Y., et al. (2018). Geochronology, geochemistry and tectonic settings of granodiorite in Lalong area, Namling, Tibet. *Earth Sci.* 43 (12), 4566–4585. doi:10.3799/dqkx.2018.271

Jia, X. H., Wang, X. D., and Yang, W. Q. (2017). Petrogenesis and geodynamic implications of the early Paleozoic potassic and ultrapotassic rocks in the south China block. *J. Asian Earth Sci.* 135, 80–94. doi:10.1016/j.jseaes.2016.12.013

Jia, X. H., Wang, X. D., and Yang, W. Q. (2022). Identification and petrogenesis of Dajin highly fractionated A-type granites formed at early Paleozoic in Dayaoshan Area of Guangxi, China. *J. Earth Sci. Environ.* 44 (2), 171–190. doi:10.19814/j.jese.2021.09048

Jiang, X. Z., Kang, Z. Q., Xu, J. F., Feng, Z. H., Pang, C. J., Fang, G. C., et al. (2017). Early Paleozoic granodioritic plutons in the Shedong W–Mo ore district, Guangxi, southern China: products of re-melting of middle Proterozoic crust due to magma underplating. *J. Asian Earth Sci.* 141, 59–73. doi:10.1016/j.jseaes.2016.11.004

Jiang, X. Z., Kang, Z. Q., Xu, J. F., Xiong, S. Q., and Wu, J. C. (2015). LA-(MC)-ICP-MS zircon U-Pb dating of porphyry from Baoshan copper deposit of Dayaoshan uplift area in Guangxi. *J. Guilin Univ. Technol.* 35 (4), 766–773. doi:10.3969/j.issn.1674-9057.2015.04.014

Laurent, A., Janousek, V., Magna, T., Schulmann, K., and Míková, J. (2014). Petrogenesis and geochronology of a post-orogenic calc-alkaline magmatic association: the Žulová Pluton, Bohemian Massif. *J. Geosciences* 59 (4), 415–440. doi:10.3190/jgeosci.176

Li, J. H. (2013). Mesozoic geotectonic process in south China. Ph.D. Thesis. Beijing, China: Chinese Academy of Geological Sciences.

Li, W., Wei, Y. F., Liao, K. L., and Yang, Z. (2014). Geochemical characteristics of granite porphyry and its relationship with mineralization in Baoshan porphyry copper deposit, Dayaoshan, Eastern Guangxi. *Geol. Mineral Resour. South China* 30 (2), 88–98. doi:10.3969/j.issn.1007-3701.2014.02.002

Li, W. J., Liang, J. C., and Feng, Z. H. (2006). Judging for characteristics of geochemical and structural environment of several Caledonian granitoids in Northeast Guangxi. *Mineral. Resour. Geol.* 20 (4–5), 353–360.

Li, X., Qi, C., Liu, Y., Liang, X., Tu, X., Xie, L., et al. (2005). Petrogenesis of the Neoproterozoic bimodal volcanic rocks along the western margin of the Yangtze Block, new constraints from Hf isotopes and Fe/Mn ratios. *Chin. Sci. Bull.* 50, 2481–2486. doi:10.1360/982005-287

Liu, L., Liu, F. L., and Cai, Y. F. (2020). Mineral feature of biotite in Da'ning rock mass in northeast Guangxi and its indication of diagenesis. *Mineral. Resour. Geol.* 34 (2), 294–301. doi:10.19856/j.cnki.issn.1001-5663.2020.02.016

Liu, L., Xiao, W. J., Liu, X. J., Zhao, Z. X., and Wang, Y. B. (2024). Early triassic S-type granitoids in the Qinzhou Bay area, south China: petrogenesis and tectonic implications. *Minerals* 14 (1), 22. doi:10.3390/min14010022

Liu, M. H., Shi, Y., Tang, Y. L., Zhao, Z. X., Liu, X. J., Gao, A. Y., et al. (2021). Petrogenesis and tectonic significance of Caledonian I-type granitoids in Southeast Guangxi, South China. *Earth Sci.* 46 (11), 3965–3992. doi:10.3799/dqkx.2021.035

Liu, Q., Pan, L. C., Wang, X. S., Yan, J., and Xing, L. Z. (2023). Apatite geochemistry as a proxy for porphyry-skarn Cu genesis: a case study from the Sanjiang region of SW China. *Front. Earth Sci.* 11, 1185964. doi:10.3389/feart.2023.1185964

Liu, Y., Xiao, Q. H., Geng, S. F., Wang, X. X., and Chen, B. H. (2010a). Magmatic mingling origin of adamellite, zircon U-Pb dating and Hf isotopes evidence of microgranular dioritic enclaves and host rocks from Yangtianu adamellite of Qitianling, South China. *Geol. China* 37 (4), 1081–1091.

Liu, Y. S., Gao, S., Hu, Z. C., Gao, C. G., Zong, K. Q., and Wang, D. B. (2010b). Continental and oceanic crust Recycling-induced melt-peridotite interactions in the trans-North China orogen: U-Pb dating, Hf isotopes and trace elements in zircons from mantle Xenoliths. *J. Petrology* 51 (1–2), 537–571. doi:10.1093/petrology/egp082

Liu, Z., Jiang, Y. H., Jia, R. Y., Zhao, P., and Zhou, Q. (2015). Origin of Late Triassic high-K calc-alkaline granitoids and their potassic microgranular enclaves from the western Tibet Plateau, northwest China: implications for Paleo-Tethys evolution. *Gondwana Res.* 27 (1), 326–341. doi:10.1016/j.gr.2013.09.022

Ludwing, K. R. (2003). *ISOPLOT 3.00, a geochronological toolkit for microsoft excel*. California: Berkeley Geochronology Center.

Lyu, P. L., Wang, Y. F., Lyu, C. L., Yang, F. Q., Shi, K., Li, H. L., et al. (2020). The nature of Early Palaeozoic Kwangsian orogenic event in the South China Block: constraints from detrital zircons in Cambrian strata. *Int. Geol. Rev.* 63 (11), 1423–1436. doi:10.1080/00206814.2020.1771781

Ma, Z. W., Guo, F., Zhao, L., Huang, X., Wen, Y. Q., and Zhang, F. (2024). Disequilibrium melting of recycled phosphate-rich crust in Yunkai Massif, South China. *Lithos* 474–475, 107592. doi:10.1016/j.lithos.2024.107592

Maniar, P. D., and Piccoli, P. M. (1989). Tectonic discrimination of granitoids. *Geol. Soc. Am. Bull.* 101 (5), 635–643. doi:10.1130/0016-7606(1989)101<0635:tdog>2.3.co;2

Mao, J. W., Cheng, Y. B., Chen, M. H., and Pirajno, F. (2013). Major types and time-space distribution of Mesozoic ore deposits in South China and their geodynamic settings. *Min. Deposita* 48, 267–294. doi:10.1007/s00126-012-0446-z

Mao, J. W., Zheng, W., Xie, G. Q., Lehmann, B., and Goldfarb, R. (2021). Recognition of a Middle-Late Jurassic arc-related porphyry copper belt along the southeast China coast: geological characteristics and metallogenic implications. *Geology* 49 (5), 592–596. doi:10.1130/g48615.1

Middlemost, E. A. K. (1985). *Magmas and magmatic rocks*. London: Longman, l–266.

Miller, C. F. (1985). Are strongly peraluminous magmas derived from pelitic sedimentary sources? *J. Geol.* 93 (6), 673–689. doi:10.1086/628995

Nitoi, E., Munteanu, M., Marice, S., Paraschivoiu, (2002). Magma enclave interactions in the east Carpathian subvolcanic zone, Romania, petrogenetic implications. *J. Volcanol. Geotherm. Res.* 118 (1–2), 229–259. doi:10.1016/s0377-0273(02)00258-5

Nong, J. N., Huang, X. Q., Guo, S. Y., Sun, M. H., Deng, B., and Zou, Y. (2017b). Discovery of Caledonian basic rocks in Dayaoshan region, eastern Guangxi and its geological significance. *Geol. Sci. Technol. Inf.* 36 (6), 113–121. doi:10.19509/j.cnki.dzkq.2017.0612

Nong, J. N., Zhou, Y., Qiu, E. L., Guo, S. Y., Ye, X. S., Xiang, F., et al. (2017a). Petrogenesis of Dacun and Gulong plutons in southeastern Guangxi: constraints from geochemistry, zircon U-Pb ages and Hf isotope. *Geol. Bull. China* 36 (2-3), 224–237. doi:10.3969/j.issn.1671-2552.2017.02.006

Nowell, G. M., Kempton, P. D., Noble, S. R., Fitton, J. G., Saunders, A. D., Mahoney, J. J., et al. (1998). High precision Hf isotope measurements of MORB and OIB by thermal ionisation mass spectrometry: insights into the depleted mantle. *Chem. Geol.* 149 (3-4), 211–233. doi:10.1016/s0009-2541(98)00036-9

Patchett, P. J., Kouvo, O., Hedge, C. E., and Tatsumoto, M. (1982). Evolution of continental crust and mantle heterogeneity, Evidence from Hf isotopes. *Contributions Mineralogy Petrology* 78, 279–297. doi:10.1007/bf00398923

Pearce, J., Harris, N. B. W., and Tindle, A. G. (1984). Trace element discrimination diagrams for the tectonic interpretation of granitic rocks. *J. Petrol.* 25 (4), 956–983. doi:10.1093/petrology/25.4.956

Peccerillo, A., and Taylor, S. R. (1976). Geochemistry of Eocene calc-alkaline volcanic rocks from the Kastamonu area, Northern Turkey. *Contrib. Min. Petrol.* 58, 63–81. doi:10.1007/bf00384745

Perugini, D., Poli, G., Christofids, G., and Eleftheriadis, G. (2003). Magma mixing in the Sithonia Plutonic Complex, Greece, evidence from mafic microgranular enclaves. *Mineral. Petrol.* 78 (3–4), 173–200. doi:10.1007/s00710-002-0225-0

Petford, N., and Gallagher, K. (2001). Partial melting of mafic (amphibolitic) lower crust by periodic influx of basaltic magma. *Earth Planet Sci. Lett.* 193 (3-3), 483–499. doi:10.1016/s0012-821x(01)00481-2

Qi, L., Hu, J., and Conrad, D. G. (2000). Determination of trace elements in granites by inductively coupled plasma mass spectrometry. *Talanta* 51 (3), 507–513. doi:10.1016/s0039-9140(99)00318-5

Qin, X. F., Wang, Z. Q., Gong, J. H., Zhao, G. Y., Shi, H., Zhan, J. Y., et al. (2017). The confirmation of Caledonian intermediate-mafic volcanic rocks in northern margin of Yunkai block: evidence for Early Paleozoic paleo-ocean basin in southwestern segment of Qinzhou-Hangzhou joint belt. *Acta Petrol. Sin.* 33 (3), 791–809. doi:10.16631/j.cnki.cn15-1331/p.2021.01.014

Qiu, J. W. (2021). Geological characteristics of Shedong tungsten polymetallic deposit in Dayao Mountains, Guangxi. *West. Resour.* 01, 44–46.

Shao, F. L., Niu, Y. L., Liu, Y., Chen, S., Kong, J., and Duan, M. (2017). Petrogenesis of triassic granitoids in the east Kunlun orogenic belt, northern Tibetan plateau and their tectonic implications. *Lithos* 282-283, 33–44. doi:10.1016/j.lithos.2017.03.002

Shu, L. S., Chen, X. Y., and Lou, F. S. (2020). Pre-Jurassic tectonics of the south China. *Acta Geol. Sin.* 94 (2), 333–360. doi:10.19762/j.cnki.dizhixuebao.2020046

Shu, L. S., Yu, J. H., Jia, D., Wang, B., and Shen, W. Z. (2008). Early Paleozoic orogenic belt in the eastern segment of South China. *Geol. Bull. China* 27 (10), 1581–1593. doi:10.3969/j.issn.1671-2552.2008.10.001

Shu, X. J., Jiang, W., Wang, D., Cheng, C., and Wang, H. Z. (2023). Origin and implication of two newly identified peraluminous A-type granites in the early Paleozoic orogeny, Southeast Asia. *Front. Earth Sci.* 11, 1137157. doi:10.3389/feart.2023.1137157

Song, M. J., Shu, L. S., Santosh, M., Li, J. Y., and Li, J. Y. (2015). Late early paleozoic and early mesozoic intracontinental orogeny in the South China craton: geochronological and geochemical evidence. *Lithos* 232, 360–374. doi:10.1016/j.lithos.2015.06.019

Souza, Z. S. D., Martin, H., Peucat, J. J., Sa, D. F. F., and Macedo, M. H. D. F. (2007). Calc-alkaline magmatism at the Archean Proterozoic transition: the caico complex basement (NE Brazil). *J. Petrology* 48 (11), 2149–2185. doi:10.1093/petrology/egm055

Sun, S. S., and McDonough, W. F. (1989). Chemical and isotopic systematics of oceanic basalts: implications for mantle composition and processes. In A. D. Saunders, and M. J. Norry (Editors). *Chemical and isotopic systematics of oceanic basalts: implications for mantle composition and processes*, (London, Special Publications). 42 (1), 313–345. doi:10.1144/gsl.sp.1989.042.01.19

Sylvester, P. J. (1998). Post-collisional strongly peraluminous granites. *Lithos* 45 (1), 29–44. doi:10.1016/s0024-4937(98)00024-3

Tang, Y. L., Shi, Y., Hu, X. M., Liu, X. J., and Huang, C. W. (2021). Petrogenesis of early paleozoic I-type granitoids in the Wuyi-Yunkai orogen, south China: implications for the tectono-magmatic evolution of the cathaysia block. *J. Asian Earth Sci.* 220, 104906. doi:10.1016/j.jseaes.2021.104906

Tang, Y. Y., Shi, Y., Weng, B. Y., Zhou, Y. X., and Lan, Y. C. (2023). Petrography, geochemistry and geochronology of igneous rocks from the Jiangnan orogen, south China: constraints on the early paleozoic tectonic evolution of the South China block. *Front. Earth Sci.* 11, 1202477. doi:10.3389/feart.2023.1202477

Thompson, M., Potts, P. J., Kane, J. S., and Wilson, S. (1999). GEOPT5-an international proficiency test for analytical geochemistry laboratories. *Rep. Round* 5, 23.

Vervoort, J. D., and Blichert-Toft, J. (1999). Evolution of the depleted mantle, Hf isotope evidence from juvenile rocks through time. *Geochim. Cosmochim. Acta* 63 (3-4), 533–556. doi:10.1016/s0016-7037(98)00274-9

Wang, T. R., Peng, H. J., Xia, Y., Chen, Y., Yang, D. J., and Zhou, Q. (2022). Magmatic processes of granitoids in the Hongniu-Hongshan porphyry-skarn copper deposit, southern Yidun Terrane, China: evidence from mineral geochemistry. *Minerals* 12 (12), 1559. doi:10.3390/min12121559

Wang, Y. J., Fan, W. M., Zhang, G. W., and Zhang, Y. H. (2013). Phanerozoic tectonics of the south China block: Key observations and controversies. *Gondwana Res.* 23 (4), 1273–1305. doi:10.1016/j.gr.2012.02.019

Wang, Y. J., Fan, W. M., Zhao, G. C., Ji, S. C., and Peng, T. P. (2007). Zircon U-Pb geochronology of gneissic rocks in the Yunkai massif and its implications on the Caledonian event in the South China Block. *Gondwana Res.* 12 (4), 404–416. doi:10.1016/j.gr.2006.10.003

Wang, Y. J., He, H. Y., Gan, C. S., and Zhang, Y. Z. (2018). Petrogenesis of the early Silurian Dashuang high-Mg basalt-andesite-dacite in eastern south China, origin from a palaeosubduction-modified mantle. *J. Geol. Soc.* 175 (6), 949–966. doi:10.1144/jgs2018-102

Wang, Y. J., Zhang, A. M., Fan, W. M., Zhao, G. C., Zhang, G. W., Zhang, Y. Z., et al. (2011). Kwangsian crustal anatexis within the eastern south China block: geochemical, zircon U-Pb geochronological and Hf isotopic fingerprints from the gneissoid granites of Wugong and Wuyi-Yunkai domains. *Lithos* 127 (1-2), 239–260. doi:10.1016/j.lithos.2011.07.027

Whalen, J. B., Currie, K. L., and Chappell, B. W. (1987). A-type granites: geochemical characteristics, discrimination and petrogenesis. *Contrib. Min. Petrol.* 95, 407–419. doi:10.1007/bf00402202

Wilson, M. (1989). *Igneous petrogenesis*. London: Allen and Unwin.

Wu, F. Y., Li, X. H., Yang, J. H., and Zheng, Y. F. (2007b). Discussions on the petrogenesis of granites. *Acta Petrol. Sin.* 23 (6), 1217–1238. doi:10.3969/j.issn.1000-0569.2007.06.001

Wu, F. Y., Li, X. H., Zheng, Y. F., and Gao, S. (2007a). Lu-Hf isotopic systematics and their applications in petrology. *Acta Petrol. Sin.* 23 (2), 185–220. doi:10.3969/j.issn.1000-0569.2007.02.001

Wu, J. C., Kang, Z. Q., Feng, Z. H., Fang, G. C., Pang, C. J., Zhang, Q. W., et al. (2015). Geochronology and geochemistry of Dacun granitic pluton in Dayaoshan uplift area. *Guangxi J. Guilin Univ. Technol.* 35 (4), 747–755. doi:10.3969/j.issn.1674-9057.2015.04.012

Xie, Y. X., Ma, L. Y., Zhao, G. C., Xie, C. F., Han, Y. G., Li, J. H., et al. (2020). Origin of the Heping granodiorite pluton: implications for syn–convergent extension and asthenosphere upwelling accompanying the Early Paleozoic orogeny in South China. *Gondwana Res.* 85, 149–168. doi:10.1016/j.gr.2020.04.002

Yang, J. H., Wu, F. Y., Wilde, S. A., Xie, L. W., Yang, Y. H., and Liu, X. M. (2007). Tracing magma mixing in granite genesis, *in situ* U-Pb dating and Hf-isotope analysis of zircons. *Contrib. Min. Petrol.* 153 (2), 177–190. doi:10.1007/s00410-006-0139-7

Yang, M. G., Huang, S. B., Lou, F. S., Tang, W. X., and Mao, S. B. (2009). Lithospheric structure and large-scale metallogenic process in Southeast China continental area. *Geo China* 36 (3), 528–543. doi:10.3969/j.issn.1000-3657.2009.03.004

Yao, W. H., Li, Z. X., Li, W. X., Wang, X. C., Li, X. H., and Yang, J. H. (2012). Post-kinematic lithospheric delamination of the Wuyi-Yunkai orogen in south China: evidence from ca. 435 Ma High-Mg basalts. *Lithos* 154, 115–129. doi:10.1016/j.lithos.2012.06.033

Ye, M., Zhang, Q. W., Hu, H. Q., Qin, Y., Yang, Q. J., Bai, L. A., et al. (2015). Chronology and geochemical characteristics of granodiorite porphyry of Dawangding rockmass in Dayaoshan area. *Guangxi J. Guilin Univ. Technol.* 35 (4), 756–765. doi:10.3969/j.issn.1674-9057.2015.04.013

Yi, L. W., Ma, C. Q., Wang, L. X., Lai, Z. X., Li, X. Y., Yang, Y. N., et al. (2014). Discovery of late ordovician subvolcanic rocks in south China: existence of subduction-related dacite from early paleozoic? *Earth Sci. J. China Univ. Geosci.* 39 (6), 637–653. doi:10.3799/dqkx.2014.061

Zhang, F. R., Shu, L. S., Wang, D. Z., Yu, J. H., and Shen, W. Z. (2009). Discussions on tectonic setting of Caledonian granitoids in the eastern segment of South China. *Earth Sci. Front.* 1, 248–260. doi:10.3321/j.issn:1005-2321.2009.01.027

Zhang, Q., Jiang, Y. H., Wang, G. C., Liu, Z., Ni, C. Y., and Qing, L. (2015). Origin of Silurian gabbros and I-type granites in central Fujian, SE China: implications for the evolution of the early Paleozoic orogen of South China. *Lithos* 216–217, 285–297. doi:10.1016/j.lithos.2015.01.002

Zhang, X. S., Xu, X. S., Xia, Y., and Liu, L. (2016b). Early Paleozoic intracontinental orogeny and post-orogenic extension in the South China Block: insights from volcanic rocks. *J. Asian Earth Sci.* 141, 24–42. doi:10.1016/j.jseaes.2016.07.016

Zhang, Y., Niu, Y. L., Hu, Y., Liu, J. J., Ye, L., Kong, J. J., et al. (2016a). The syn-collisional granitoid magmatism and continental crust growth in the west Kunlun orogen, China: evidence from geochronology and geochemistry of the Arkarz pluton. *Lithos* 245, 191–204. doi:10.1016/j.lithos.2015.05.007

Zhang, Z. Q., Bagas, L., Mao, J. W., Chen, M. H., and Fu, B. (2018). Mineralization associated with the fractionated cretaceous baoshan monzogranite: tectonic implications for south China. *Ore Geol. Rev.* 102, 791–910. doi:10.1016/j.oregeorev.2018.08.008

Zhou, X. M. (2003). My thinking about granite geneses of south China. *Geol. J. China Univ.* 9 (4), 556–565. doi:10.3969/j.issn.1006-7493.2003.04.009

Zhou, Y. X., Shi, Y., Huang, C. W., Liu, X. J., Lan, Y. C., Tang, Y. Y., et al. (2023). Petrogenesis and tectonic significance of Caledonian I-type granitoids in the Gulong and Liandong plutons in southeastern Guangxi. *Earth Sci. Front.* 31 (02), 224–248. doi:10.13745/j.esf.sf.2023.2.62

Zhu, J. C., Wang, R. C., Zhang, P. H., Xie, C. F., Zhang, W. L., Zhao, K. D., et al. (2009). Zircon U-Pb geochronological framework of Qitianling granite batholith, middle part of Nanling Range, South China. *Sci. China (Series D.)* 52 (9), 1279–1294. doi:10.1007/s11430-009-0154-4

Zorpi, M. J., Coulon, C., Orsini, J., and Cocirta, C. (1989). Magma mingling, zoning and emplacement in calc-alkaline granitoid plutons. *Tectonophysics* 157, 315–329. doi:10.1016/0040-1951(89)90147-9